

Selection bias in dynamically-measured super-massive black hole samples: its consequences and the quest for the most fundamental relation

Francesco Shankar^{1*}, Mariangela Bernardi², Ravi K. Sheth², Laura Ferrarese³, Alister W. Graham⁴, Giulia Savorgnan⁴, Viola Allevato⁵, Alessandro Marconi⁶, Ronald Läsker⁷, Andrea Lapi^{8,9}

¹ *Department of Physics and Astronomy, University of Southampton, Highfield, SO17 1BJ, UK*

² *Department of Physics and Astronomy, University of Pennsylvania, 209 South 33rd St, Philadelphia, PA 19104*

³ *Herzberg Institute of Astrophysics, National Research Council of Canada, Victoria, BC V9E 2E7, Canada*

⁴ *Centre for Astrophysics and Supercomputing, Swinburne University of Technology, Hawthorn, Victoria 3122, Australia*

⁵ *Department of Physics, University of Helsinki, Gustaf Hållströmin katu 2a, FI-00014 Helsinki, Finland*

⁶ *Universit degli Studi di Firenze, Dipartimento di Fisica e Astronomia, via G. Sansone 1, 50019 Sesto F.no, Firenze, Italy*

⁷ *Max Planck Institute for Astronomy, Königstuhl 17, D-69117 Heidelberg, Germany*

⁸ *SISSA, Via Bonomea 265, 34136 Trieste, Italy*

⁹ *Dip. Fisica, Univ. “Tor Vergata”, Via Ricerca Scientifica 1, 00133 Roma, Italy*

ABSTRACT

We compare the set of local galaxies having dynamically measured black holes with a large, unbiased sample of galaxies extracted from the Sloan Digital Sky Survey. We confirm earlier work showing that the majority of black hole hosts have significantly higher velocity dispersions σ than local galaxies of similar stellar mass. We use Monte-Carlo simulations to illustrate the effect on black hole scaling relations if this bias arises from the requirement that the black hole sphere of influence must be resolved to measure black hole masses with spatially resolved kinematics. We find that this selection effect artificially increases the normalization of the $M_{\text{bh}}-\sigma$ relation by a factor of at least ~ 3 ; the bias for the $M_{\text{bh}}-M_{\text{star}}$ relation is even larger. Our Monte Carlo simulations and analysis of the residuals from scaling relations both indicate that σ is more fundamental than M_{star} or effective radius. In particular, the $M_{\text{bh}}-M_{\text{star}}$ relation is mostly a consequence of the $M_{\text{bh}}-\sigma$ and $\sigma-M_{\text{star}}$ relations, and is heavily biased by up to a factor of 50 at small masses. This helps resolve the discrepancy between dynamically-based black hole-galaxy scaling relations versus those of active galaxies. Our simulations also disfavour broad distributions of black hole masses at fixed σ . Correcting for this bias suggests that the calibration factor used to estimate black hole masses in active galaxies should be reduced to values of $f_{\text{vir}} \sim 1$. Black hole mass densities should also be proportionally smaller, perhaps implying significantly higher radiative efficiencies/black hole spins. Reducing black hole masses also reduces the gravitational wave signal expected from black hole mergers.

Key words: (galaxies:) quasars: supermassive black holes – galaxies: fundamental parameters – galaxies: nuclei – galaxies: structure – black hole physics

1 INTRODUCTION

The presence of nuclear supermassive black holes (hereafter black hole) in the majority of local galaxies has become an accepted paradigm. Indeed, nuclear kinematics of a number of nearby galaxies show the clear signature of a central mass concentration, beyond what can be attributed to the observed stellar population

in the nuclear regions. Black hole masses, M_{bh} , are found to correlate with several global properties of their host galaxies (see, e.g., Ferrarese & Ford 2005; Shankar 2009; Kormendy & Ho 2013; Graham 2016, for reviews), including the stellar and/or bulge mass, velocity dispersion, σ , luminosity, light concentration or Sérsic index (e.g., Magorrian et al. 1998; Richstone et al. 1998; Ferrarese & Merritt 2000; Gebhardt & et al. 2000; Graham et al. 2001; Graham & Driver 2007a; Marconi & Hunt 2003; Häring & Rix 2004; Graham 2007; Satyapal et al. 2008;

* E-mail: F.Shankar@soton.ac.uk

Graham 2012; Kormendy & Ho 2013; McConnell & Ma 2013; Scott et al. 2013; Lasker et al. 2014; Savorgnan & Graham 2015a; Savorgnan et al. 2016; Saglia et al. 2016), and the mass of the surrounding dark matter halo (e.g., Ferrarese 2002a; Baes et al. 2003; Bogdan & Goulding 2015; Sabra et al. 2015). However, while it is true that the number of dynamical black hole mass measurements has increased over the years, such samples still remain relatively small, of the order of $\sim 70 - 80$ galaxies. This is due primarily to the difficulty of carrying out direct measurements with the required depth and spatial resolution (see, e.g., Faber 1999; Ferrarese & Ford 2005, for reviews on the challenges encountered in these observational campaigns).

Understanding the origin and reliability of these correlations is vital if we want to ultimately improve our understanding of galaxy-black hole (co-)evolution. For instance, the normalization and slope of the $M_{\text{bh}}-\sigma$ relation may contain key information on whether feedback is primarily via energy or momentum transfer (e.g., Silk & Rees 1998; Fabian 1999; King 2005; Wyithe & Loeb 2005; Fabian 2012; King 2014). Directly related to the normalization of the black hole scaling relations is the value of the virial f_{vir} -factor used to derive the masses of black holes probed via reverberation mapping studies (Onken et al. 2004; Vestergaard & Peterson 2006). If the $M_{\text{bh}}-\sigma$ normalization is too high by some amount, then the f_{vir} -factor will be too high by this same amount. Shifting the normalization to lower masses will not only lower the quasar masses inferred at high- z , thus helping to solve the problem of the time required to grow the black hole by accretion, but an abundance of lower-mass black holes, now with $M_{\text{bh}} < 10^5 M_{\odot}$ (e.g., “intermediate mass black holes”), will be realized, joining the ranks of objects like HLX-1 in ESO 243-49 (Farrell et al. 2009, 2014; Webb et al. 2014) and NGC 2276-3c (Mezcua et al. 2015).

The normalization of the $M_{\text{bh}}-M_{\text{bulge}}$ relation is also a key ingredient in predicting what pulsar timing array searches (e.g., Sesana et al. 2008; Hobbs et al. 2010; Sesana 2013; Kramer & Champion 2013; Rosado & Sesana 2014; Rosado et al. 2015) for gravitational radiation will see (Bonnor & Rotenberg 1961; Peres 1962; Bekenstein 1973; Buonanno & Damour 2000; Berti et al. 2009). With the normalizations currently in use, the pulsar timing arrays were expected to have detected a gravitational wave background (Shannon et al. 2013, 2015). To explain the lack of detection, theorists have begun to consider new possibilities, like rather eccentric orbits for the coalescing binary supermassive black hole population so as to shift the gravitational wave spectral energy distribution out of the observing window of pulsar timing arrays. However, eccentric orbits are at odds with the observed ellipticities of partially-depleted cores (see, e.g., Dullo & Graham 2015). Environmental effects are also being invoked to reduce the time over which the binary emits gravitational radiation, and thus possibly resolve the dilemma (e.g., Ravi et al. 2014). However, if the $M_{\text{bh}}-M_{\text{bulge}}$ normalization on which these arguments are based is too high, then the expected gravitational wave signal has been overestimated.

Scatter in the black-hole galaxy scaling relations is thought to bear imprints of the amount of collisionless “dry mergers” experienced by the (most massive) hosts (e.g., Boylan-Kolchin et al. 2006; Peng 2007; Hirschmann et al. 2010; Jahnke & Maccio 2011, but see Savorgnan & Graham 2015a). The Sersic index and the presence of a partially depleted core, along with their possible correlations with the mass of the central black hole, are also believed to contain information about the types of mergers responsible for shaping the host spheroids (e.g., Aguerri et al. 2001; Merritt 2006; Hilz et al. 2013; Graham & Scott 2013, 2015).

Beyond the local universe, data tracking the evolution of active and star-forming galaxies over cosmic time shows that black hole accretion and star formation peak at similar epochs (e.g., Marconi et al. 2004; Merloni 2004; Silverman et al. 2008; Zheng et al. 2009; Shankar et al. 2009b; Delvecchio et al. 2014), consistent with the idea that massive black holes and their host galaxies may be co-evolving. One way to test this co-evolution is by exploring the cosmic evolution of the above scaling relations. Thus, the characterization of the scaling relations of black holes with their hosts is the subject of intense observational efforts, both locally and at high redshift (e.g., Shields et al. 2006; Lauer et al. 2007b; Treu et al. 2007; Woo et al. 2008; Gaskell & Kormendy 2009; Shankar et al. 2009a; Merloni et al. 2010; Schulze & Wisotzki 2011; Falomo et al. 2014; Shen et al. 2015).

In-depth knowledge of the black hole-host scaling relations at any epoch can also potentially provide statistical clues on the mass densities of black holes. For instance, a robust estimate of the black hole mass function can provide valuable constraints on the mechanisms governing black hole growth over cosmic time, such as mergers or disc instabilities (e.g., Kauffmann & Haehnelt 2000; Vittorini et al. 2005; Bower et al. 2006; Fontanot et al. 2006; Lapi et al. 2006; Menci et al. 2006; Malbon et al. 2007; Shankar et al. 2009b; Bournaud et al. 2011; Fanidakis et al. 2011; ?; Dubois et al. 2013; Hirschmann et al. 2014; Sesana et al. 2014; Aversa et al. 2015; Fontanot et al. 2015; Sijacki et al. 2015), as well as on the average radiative efficiencies/black hole spin and/or fraction of obscured sources (e.g., Soltan 1982; Elvis et al. 2002; Shankar et al. 2013b; Aversa et al. 2015; Tucci & Volonteri 2016). However, because direct dynamical measurements of black hole masses are difficult to obtain, considerable effort has been invested in identifying easily observed proxies for M_{bh} . As an example, the standard procedure for calculating the black hole “mass function” has been to assume that all galaxies host black holes, and to use the correlation between the observable proxy and M_{bh} to transform the observed distribution of the proxy into a distribution of M_{bh} (e.g., Salucci et al. 1999; Aller & Richstone 2002; Ferrarese 2002b; McLure & Dunlop 2004; Marconi et al. 2004; Shankar et al. 2004; Benson et al. 2007; Tundo et al. 2007; Graham et al. 2007; Yu & Lu 2008; Vika et al. 2009).

This procedure rests on the assumption that one has correctly identified the observable proxy for M_{bh} , and that the scaling relation used to convert from it to M_{bh} has been correctly estimated. For example, the two most commonly used proxies, stellar velocity dispersion and bulge luminosity, lead to rather different estimates of $\phi(M_{\text{bh}})$ (e.g., Lauer et al. 2007a; Tundo et al. 2007, but see also Graham 2008): the luminosity-based estimate predicts many more massive black holes. To date, there is no consensus on which is correct, at least for the more massive galaxies. There is also no consensus on whether or not the best proxy for M_{bh} involves more than one observable. For example, some groups (e.g. Feoli & Mele 2005; Hopkins et al. 2007) argue that $M_{\text{bh}} \propto R^{2-\beta/2} \sigma^{\beta}$, with R any characteristic (e.g., half-light) radius of the host galaxy and $\beta \approx 3$, whereas, on the basis of more recent samples, Beifiori et al. (2012) report no compelling evidence for anything other than $M_{\text{bh}} \propto \sigma^{\beta}$ with $\beta \approx 4$, in line with Graham (2008). Notice that the second parameter in the Feoli & Mele (2005) formulation becomes less important when $\beta \rightarrow 4$.

However, the two issues above are coupled: one cannot properly address the observable proxy question if the scaling relations have been incorrectly estimated. While there exists a wealth of literature on measuring these relations in the local dynamical black hole samples (e.g., Ford et al. 1998; Yu & Tremaine 2002;

Novak et al. 2006; Lauer et al. 2007b; Graham 2007; Batcheldor 2010; Merloni et al. 2010; Graham et al. 2011; Beifiori et al. 2012; Graham & Scott 2013; Schulze & Wisotzki 2014), the extent to which selection effects can bias these estimates has not been fully addressed. This matters because, as pointed out by Bernardi et al. (2007) almost a decade ago, the available black hole samples are not a representative subset of early-type galaxies: their host galaxies have larger than expected velocity dispersions than early type galaxies of the same luminosity or stellar mass. Although Yu & Tremaine (2002) had also noted that σ - L in black hole samples appeared to be biased – and van den Bosch et al. (2015) have recently reconfirmed that black hole hosts tend to be the densest galaxies given their luminosity – they ignored the implications for black hole scaling relations. Bernardi et al. (2007) used analytic arguments and Monte-Carlo simulations to show that this is unwise – selection effects can heavily bias black hole scaling relations.

There is at least one obvious selection effect: direct black hole mass estimates depend on resolving (at least approximately) the sphere of influence $r_{\text{infl}} \equiv GM_{\text{bh}}/\sigma^2$ of the black hole (e.g. Peebles 1972; Ford et al. 1998; Merritt & Ferrarese 2001a; Barth 2004; Batcheldor 2010; Graham et al. 2011; Gültekin et al. 2011). This, at fixed signal-to-noise ratio, becomes more difficult as the distance to the black hole increases. The first part of this paper is devoted to a study of this selection effect. In the second, we address the question of which scaling relation is more fundamental.

When cosmological parameters are necessary, we set $h = 0.7$, $\Omega_m = 0.3$, $\Omega_\Lambda = 0.7$.

2 DATA

The galaxy sample used as the reference data in this study is the one collected and studied in Meert et al. (2015), and we refer to that paper for full details. Briefly, galaxies are selected from the Sloan Digital Sky Survey (SDSS) DR7 spectroscopic sample (Abazajian et al. 2009) in the redshift range $0.05 < z < 0.2$, and with a morphology classification based on the Bayesian automated morphological classifier by Huertas-Company et al. (2011). The latter statistically quantifies the morphological appearance of a galaxy with probabilities $p(\text{E-S0})$ of being an elliptical (E), a lenticular (S0), and a spiral, based on several different criteria. Unless otherwise noted, we will always define the sample of ellipticals/lenticulars as those SDSS galaxies with a $p(\text{E-S0}) > 0.80$, though the exact cut chosen to select early-type galaxies in SDSS does not impact any of our conclusions.

Galaxy mass-to-light ratios are linear functions of colour (following Bell et al. 2003; see Equation 6 in Bernardi et al. 2010), derived through Spectral Energy Distribution fitting using the Bruzual & Charlot (2003) synthesis population models, and converted to a Chabrier (2003) Initial Mass Function (IMF). Stellar masses are obtained by multiplying these mass-to-light ratios by the luminosity. Bernardi et al. (2013, 2014, 2016b) have emphasized that the choice of luminosity matters as much as the choice of IMF. They provide three different estimates for the stellar masses: one based on the SDSS CMODEL magnitude; another, based on fitting a single Sérsic profile Sérsic (1963); and a third, SEREXP, based on a combination of Sérsic and exponential light profiles. Unless we specify otherwise, all (circularized) galaxy effective radii and luminosities – and hence stellar masses – which follow are based on their SEREXP fits (also see Meert et al. 2015). While this choice matters quantitatively, it makes no qualitative difference to our findings. In addition, each of the groups we discuss below uses a dif-

ferent way of estimating M_{star} (assumptions about star formation history, dust, etc...). In principle, we should correct all to a common reference point. However, once corrected to the same IMF, systematic biases in stellar masses are of order ~ 0.1 dex Bernardi et al. (2016a), and our results are robust to these small shifts, so we have not applied any changes (other than to scale to a common IMF).

We will consider five different black hole samples¹: those of Savorgnan et al. (2016), Läsker et al. (2014), McConnell & Ma (2013), Beifiori et al. (2012), and Saglia et al. (2016). The other five samples are based on the same sample of local galaxies with dynamical mass measurements of the central black hole, but with different estimates of the host galaxy velocity dispersion and luminosity.

The sample of Savorgnan et al. (2016) is the largest, most up-to-date set of galaxies with dynamically measured black holes. It consists of 66 galaxies with dynamical estimates of their black hole masses as reported by Graham & Scott (2013) or Rusli et al. (2013). Using 3.6μ (Spitzer satellite) images, Savorgnan & Graham (2015b) modelled the one-dimensional surface brightness profile (measured along the major-axis and also the equivalent-circularized axis, i.e. the “circularized” profile) of each one of these 66 galaxies and estimated the structural parameters of their spheroidal component by simultaneously fitting a Sérsic function (used to describe the spheroid) in combination with additional components such as bars, discs, rings, nuclei. When available, kinematic information was used to confirm the presence and radial extent of rotating discs in the early-type galaxies.

Galaxy luminosities were converted into stellar masses assuming a Chabrier IMF and adopting a constant mass-to-light ratio of $(M/M_\odot)/(L/L_\odot) = 0.6$ from Meidt et al. (e.g. 2014). Savorgnan et al. (2016) also explored more sophisticated ways of computing stellar masses based on colours, finding similar results. The total galaxy effective radii (measured along the major- and the equivalent-axis) were estimated from the one-dimensional cumulative distribution of light as a function of galaxy radius, i.e., by imposing that the observed surface brightness profile integrated from $R = 0$ to $R = R_e$ equal half of the total brightness. To these galaxy radii we assign a typical average uncertainty of 0.1 dex. Central velocity dispersions are all derived from Hyperleda. In the following we exclude from their original sample NGC3842, NGC4889, UGC3789, and IC2560 which do not have Hyperleda velocity dispersions. We also remove another 10 galaxies that Kormendy & Ho (2013) classify either as ongoing mergers or as having uncertain black hole mass estimates (see their Tables 2 and 3). Finally, we do not consider the four galaxies for which Savorgnan et al. (2016) report only upper limits to the total magnitude (see their Table 1). This limits the final sample to 48 galaxies, of which 37 are E-S0 galaxies.

The photometry characterizing the Läsker et al. (2014) sample of 35 galaxies, selected among those available in the literature with “secure” dynamical black hole mass measurements, was determined from deep, high spatial resolution images obtained from the wide-field WIRCam imager at the Canada–France–Hawaii–Telescope, accompanied by dedicated sky subtraction and improved fitting techniques similar to those by Savorgnan & Graham (2015b). To make a closer comparison with the other black hole samples and SDSS galaxies we adopt as a reference their stan-

¹ We do not show results from Kormendy & Ho (2013) because their photometry is not as accurate as the others and they do not provide effective radii.

standard Sérsic plus exponential luminosities, but note that using their “improved” luminosities – based on more complex fitting models that may include additional components other than bulge and disc – does not alter our conclusions. We convert their K -band luminosities into stellar masses assuming a Chabrier IMF adopting an average standard mass-to-light ratio of $(M/M_\odot)/(L/L_\odot) = 0.67$ (e.g., Longhetti & Saracco 2009). Velocity dispersions are all taken from Hyperleda.

From the original sample of McConnell & Ma (2013) we retain only those objects which Kormendy & Ho (2013) label as secure, and further restrict to those with 3.6μ luminosities and effective radii derived from Sérsic plus exponential fits by Sani et al. (2011). This reduces the original sample to 34 galaxies, of which 26 are E–S0s. We adopt their velocity dispersions obtained from integration of the spatially resolved measurements of the line-of-sight velocity dispersion and radial velocity from the sphere of influence of the black hole to one effective radius. The latter definition can reduce the values of central velocity dispersion by 10%–15% but, according to McConnell & Ma (2013), more accurately reflects the global structure of the host galaxy and is less sensitive to angular resolution.

The structural parameters in Beifiori et al. (2012) are also homogeneously derived from bulge-to-disc decompositions of SDSS i -band images. Stellar masses were derived from adopting the mass-to-light ratio versus colour relations by Bell et al. (2003), who in turn adopted a “diet” Salpeter IMF, which yields about 0.15 dex higher stellar masses than a Chabrier IMF (e.g., Bernardi et al. 2010). Stellar velocity dispersions come either from Beifiori et al. (2009) or Gültekin et al. (2009) and are rescaled to a velocity dispersion σ equivalent to an effective stellar dispersion, measured within a circular aperture of radius R_e . When showing correlations with black hole mass, we will restrict to the subsample of galaxies by Beifiori et al. (2012) with updated black hole masses from Kormendy & Ho (2013).

To couple these datasets with SDSS galaxies, we convert SDSS velocity dispersions from $R_e/8$ to R_e using the mean aperture corrections in Cappellari et al. (2006):

$$\left(\frac{\sigma_R}{\sigma_e}\right) = (R/R_e)^{-0.066}. \quad (1)$$

When dealing with the velocity dispersions σ_{HL} from the Hyperleda database (Paturel et al. 2003), in which all measurements have been homogenized to a common aperture of 0.595 kpc, we also correct according to Equation 1. These corrections are relatively small, and are not crucial for our results. The aperture correction in Equation 1 is consistent with other independent works (e.g., Jorgensen et al. 1996). Cappellari et al. (2013) claim a slight mass-dependent aperture correction, as expected in pressure-supported systems (Graham & Colless 1997), though still, on average, in good agreement with Equation 1.

While our work was being reviewed for publication, Saglia et al. (2016) reported results from the SINFONI black hole survey. For completeness, we briefly report results derived from their sample in Section 4.6 and Appendix A. Bulge luminosities and half-light radii provided with this sample are determined from photometric decompositions that include bulges, discs, bars and rings. Bulge luminosities are then converted to stellar masses via dynamically determined mass-to-light ratios, and velocity dispersions are computed as line-of-sight weighted means within one effective radius. We remove from this sample 11 galaxies classified as unreliable by Kormendy & Ho (2013).

3 SELECTION BIAS

Bernardi et al. (2007), and more recently van den Bosch et al. (2015), noted that the scaling relations defined by the early-type galaxy hosts for which dynamically measured black hole masses are available differ from those of the early-type population as a whole: black hole hosts tend to have larger velocity dispersions than early type galaxies of the same luminosity. Figure 1 shows that this bias is still present in the four more recent compilations/determinations (different panels) described in the previous section. The solid line with grey bands shows the velocity dispersion σ –total stellar mass M_{star} relation of SDSS galaxies having probability $p(\text{E–S0}) > 0.80$ of being classified as ellipticals and/or lenticulars according to the Bayesian automated classification of Huertas-Company et al. (2011). The symbols in each panel show the E–S0 galaxies with dynamically measured black hole masses: in all panels, they lie significantly above the relation defined by the full SDSS. We note that the SerExp decompositions assign larger luminosities to the galaxies with the highest velocity dispersions (e.g. Bernardi et al. 2013, 2014, 2016b), thus further curving the σ – M_{star} relation (and related bias) with respect to previous estimates based on deVaucouleur’s luminosities (e.g., Tundo et al. 2007; Bernardi et al. 2010, 2011).

Graham (2008) argued that the bias discussed by Bernardi et al. (2007) was almost entirely due to lenticular and/or barred galaxies. However, an error in Figure 7 of that paper invalidates this conclusion. To double-check, the orange symbols in each panel of our Figure 1 show lenticulars: the larger bias is evident in the McConnell & Ma (2013, upper left) and Savorgnan et al. (2016, upper right) samples, but is less obvious in the bottom right panel. Even if these objects are excluded, there is a clear offset from the relation defined by the SDSS galaxies. Indeed, in the Beifiori et al. (2012) sample (bottom left) we have excluded all barred galaxies, and still find a clear offset. The offsets are evident whatever the exact sample considered, the selection adopted, the possible differences in estimating stellar masses in each subsample, and the aperture within which the velocity dispersion was estimated. In Section 4.6 we show there is also a clear offset if one considers bulge instead of total stellar masses (the SEREXP decompositions provide B/T estimates for the SDSS sample).

If the offset is a physical effect – only the densest galaxies host black holes (e.g., Saglia et al. 2016) – then it compromises the fundamental assumption in black hole demographic studies based on proxies: that all galaxies host black holes. However, there is a well-known selection effect: black hole dynamical mass estimates are only possible if (some multiple of) the black hole’s sphere of influence²,

$$r_{\text{infl}} \equiv GM_{\text{bh}}/\sigma^2, \quad (2)$$

has been resolved (e.g., Peebles 1972; Merritt & Ferrarese 2001a; Barth 2004; Batcheldor 2010; Gültekin et al. 2011; Graham & Scott 2013). Only within r_{infl} (Keplerian) dynam-

² Strictly speaking, the black hole sphere of influence depends on the exact stellar profile of the host galaxy and should thus be defined as the radius where $GM_{\text{bh}}/r = GM_{\text{star}}(< r)/r$. For a singular isothermal sphere, $GM_{\text{star}}(< r)/r = \sigma^2$ for all r , so this yields Equation 2. We have checked, however, that increasing or decreasing r_{infl} by a factor of 3 has a relatively minor impact on our conclusions. Significantly larger values of r_{infl} would tend to reduce the bias we study in this paper – but they are not supported by observations.

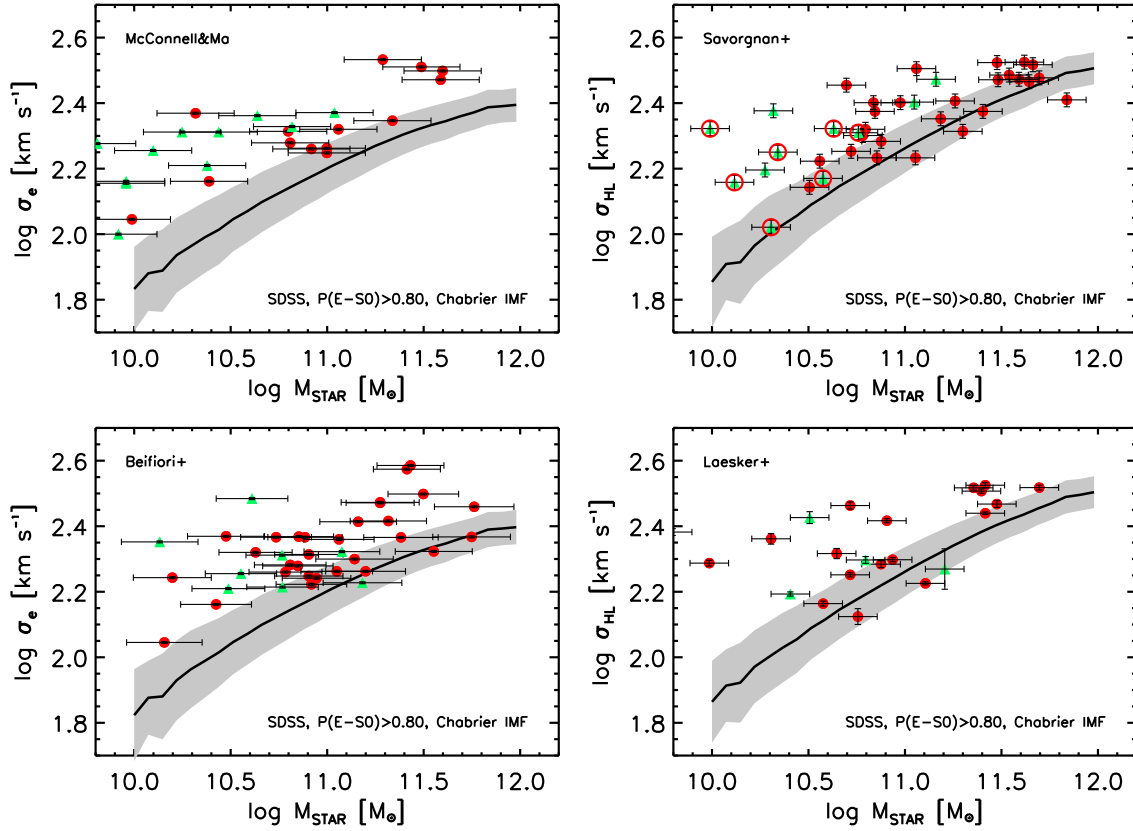


Figure 1. Mean velocity dispersion σ at a given aperture (solid lines with gray bands), as labelled on the y -axis, as a function of the total stellar mass of SDSS galaxies with a probability $p(E-S0) > 0.80$ of being classified as ellipticals and/or lenticulars (see text for details). The solid line in each panel shows the mean relation in the SDSS, based on the SEREXP stellar masses of Meert et al. 2015; gray band shows the dispersion around the mean. The symbols show the local E-S0 galaxies with dynamically measured black hole masses from McConnell & Ma (2013, top, left), Savorgnan et al. (2016, top right), Beifiori et al. (2012, bottom left), and Läscher et al. (2014, bottom right). Filled red circles in each panel show ellipticals; green triangles show lenticulars. Open circles in the upper right panel mark the galaxies classified as barred by Savorgnan et al. (2016). In all panels, most black hole hosts lie above the relations defined by the local population of SDSS galaxies regardless of morphological type.

ics is expected to be dominated by the black hole (e.g., Merritt & Ferrarese 2001b), and not adequately resolving the sphere of influence could significantly bias black hole mass estimates (e.g., Merritt 2013). The next section explores the consequences of this selection effect.

4 PROBING BLACK HOLE-GALAXY CORRELATIONS AND RESIDUALS THROUGH TARGETED MONTE CARLO TESTS

We now describe the results of Monte Carlo simulations we have performed to study how the requirement that

$$\theta_{\text{infl}} \equiv r_{\text{infl}}/d_{\text{Ang}} \quad (3)$$

where d_{Ang} is the angular diameter distance, must exceed some critical angle θ_{crit} , impacts black hole and black hole-host scaling relations. To illustrate our results, we set $\theta_{\text{crit}} = 0.1''$, a characteristic resolution limit for space-based (Hubble space telescope) observations. We have verified that none of our conclusions is significantly changed if we increase the critical radius to, say, $\theta_{\text{crit}} = 0.5''$, which is more typical for ground-based measurements. Of course, increasing θ_{crit} decreases the number of detectable objects. In addition, the bias does not scale linearly with θ_{crit} so a weak trend with resolution is expected. Finally, we stress

that this may not be the only selection effect in real samples; our goal is to study this effect in isolation.

4.1 Setting up the simulations

Our simulations, which follow the approach of Bernardi et al. (2007), work as follows:

- (i) A comoving distance d_{Com} is drawn from a distribution which is uniform in comoving volume out to 200 Mpc^3 . This cut-off is small enough that the difference between d_{Ang} and d_{Com} is irrelevant.
- (ii) A (total) stellar mass M_{star} is assigned from the Bernardi et al. (2013) stellar mass function of ellipticals+lenticulars.
- (iii) A velocity dispersion is determined by drawing from a Gaussian distribution with mean and scatter as derived from the $\sigma - M_{\text{star}}$ relation in the SDSS shown in the right panels of Figure 1.

³ This value was chosen to broadly match the outermost distance for dynamical measurements of black holes (e.g., Cygnus A, Kormendy & Ho 2013). Reducing it to 100-150 Mpc does not qualitatively change any of our conclusions.

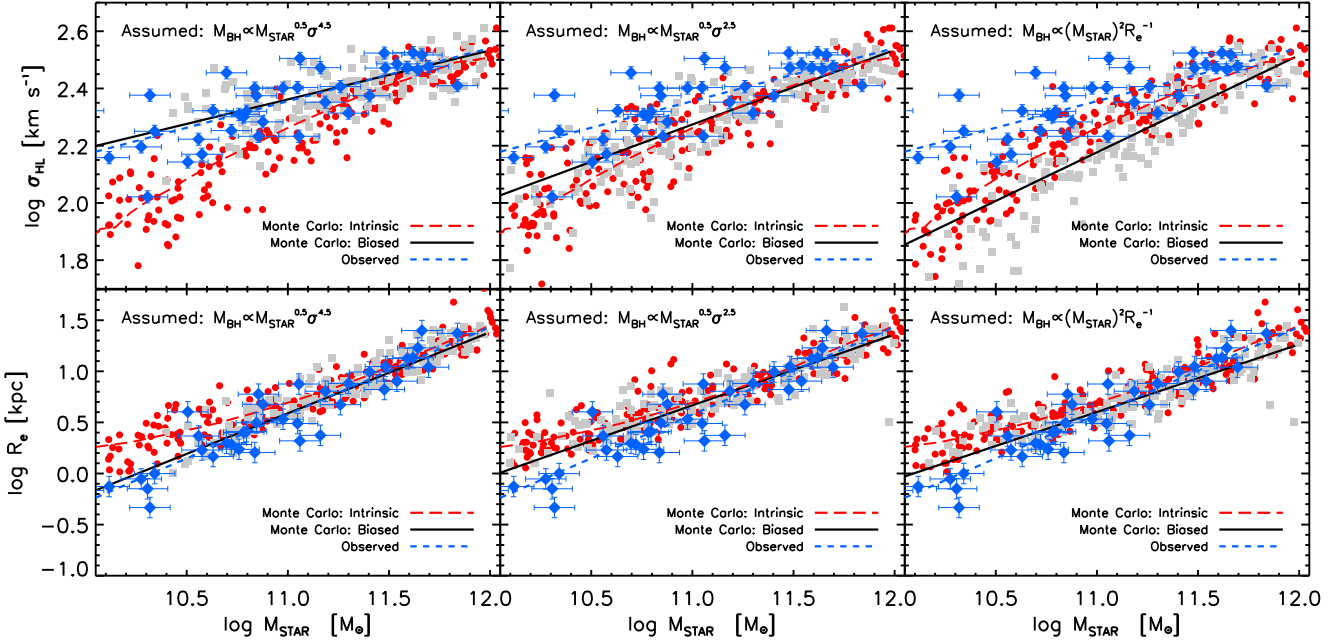


Figure 2. Host galaxy velocity dispersion (top) and effective radius (bottom) as a function of total stellar mass in Models I (left), II (middle) and III (right) for which $M_{\text{bh}} \propto M_{\text{star}}^{0.5} \sigma^{4.5}$, $M_{\text{star}}^{0.5} \sigma^{2.5}$ and M_{star}^2 / R_e , respectively. Red circles and grey squares show a random subsample of 200 objects from the full sample, and the subset which is biased by the requirement that $r_{\text{infl}} \geq 0.1''$, respectively. Long-dashed red lines show the intrinsic relations in the full sample; solid black lines show linear fits to the selection biased subsample. Blue diamonds with error bars show the dataset of Savorgnan et al. (2016), and dashed blue lines show the associated straight line fits.

(iv) The galaxy effective radii are set equal to those of the SDSS galaxy with the closest M_{star} and σ .

(v) Finally, a black hole mass is assigned to each galaxy in one of the following three ways (we discuss other possibilities in Section 4.7). In Models I and II,

$$\log \frac{M_{\text{bh}}}{M_{\odot}} = \gamma + \beta \log \left(\frac{\sigma}{200 \text{ km s}^{-1}} \right) + \alpha \log \left(\frac{M_{\text{star}}}{10^{11} M_{\odot}} \right), \quad (4)$$

with $(\gamma, \beta, \alpha) = (7.7, 4.5, 0.5)$ for Model I and $(\gamma, \beta, \alpha) = (7.75, 2.5, 0.5)$ for Model II. In Model III,

$$\log \frac{M_{\text{bh}}}{M_{\odot}} = \gamma + \beta \log \left(\frac{R_e}{5 \text{ kpc}} \right) + \alpha \log \left(\frac{M_{\text{star}}}{10^{11} M_{\odot}} \right), \quad (5)$$

with $(\gamma, \beta, \alpha) = (7.4, -1, 2)$. For all three models, we add 0.25 dex rms (Gaussian) scatter around the assumed mean relation.

(vi) We repeat the steps above many times to create what we call the full black hole sample.

(vii) For each object in the full sample we define θ_{infl} following equation (3). The subset of objects with $\theta_{\text{infl}} \geq \theta_{\text{crit}}$ make up our selection-biased sample.

Model II was chosen because it is similar to the observed (selection biased) scaling reported in the literature (e.g., Hopkins et al. 2007; Kormendy & Ho 2013; McConnell & Ma 2013). Model I has a stronger intrinsic dependence on σ which we argue later is required to explain all the observed correlations. And Model III was chosen mainly because it scales like the potential energy, so σ does not play a fundamental role; rather, in this model, the $M_{\text{bh}}-\sigma$ correlation is a result of more fundamental correlations with M_{star} and R_e . While our choices for the intrinsic scatter are close to those reported in the literature, for reasons that will become clear later, the normalizations γ in all the three models above are $\sim 0.4 - 0.6$ dex ($\sim 2.5 - 4\times$) lower than the values given in the literature.

Notice that we do not distinguish between intrinsic scatter and observational errors in our Monte Carlo simulations: we return to this later. In addition, while all the mock-based results that follow are presented in terms of total stellar mass, using bulge stellar masses (and radii) instead yields qualitatively similar results (see Section 4.6).

4.2 The selection biased $\sigma-M_{\text{star}}$ and R_e-M_{star} relations

In this section we answer the basic question: can the r_{infl} -selection effect help explain the discrepancy shown in Figure 1? We will use “scaling relations” to address this. In all cases, this means we treat the quantity plotted on the y -axis as the dependent variable when fitting. We never treat it as the independent variable, nor do we perform ‘bisector’-like fits. When fitting straight lines to the data, we have compared three different linear regression algorithms finding very similar results. The values we report have been performed with the IDL routine `robust_linfit`.

In the next two figures, red circles and grey squares show 200 randomly chosen members of the intrinsic and selection biased Monte-Carlo samples, and blue symbols with error bars show the E+S0s in the Savorgnan et al. (2016) dataset. Long-dashed red curves show the intrinsic scaling relations, solid black lines show linear fits to the selection biased sample, and short-dashed blue lines show linear fits to the data.

The top panels of Figure 2 show the $\sigma-M_{\text{star}}$ relation: left, middle, and right-hand panels show results for Models I, II and III. There is a clear offset between the intrinsic and selection biased objects in the top left panel, a smaller one in the top middle, and a bias in the opposite sense in the top right panel. This is easy to understand: In Model II, $r_{\text{infl}} \propto (M_{\text{star}} \sigma)^{0.5}$ is nearly a function of M_{star} only (the range of M_{star} values is much broader than of

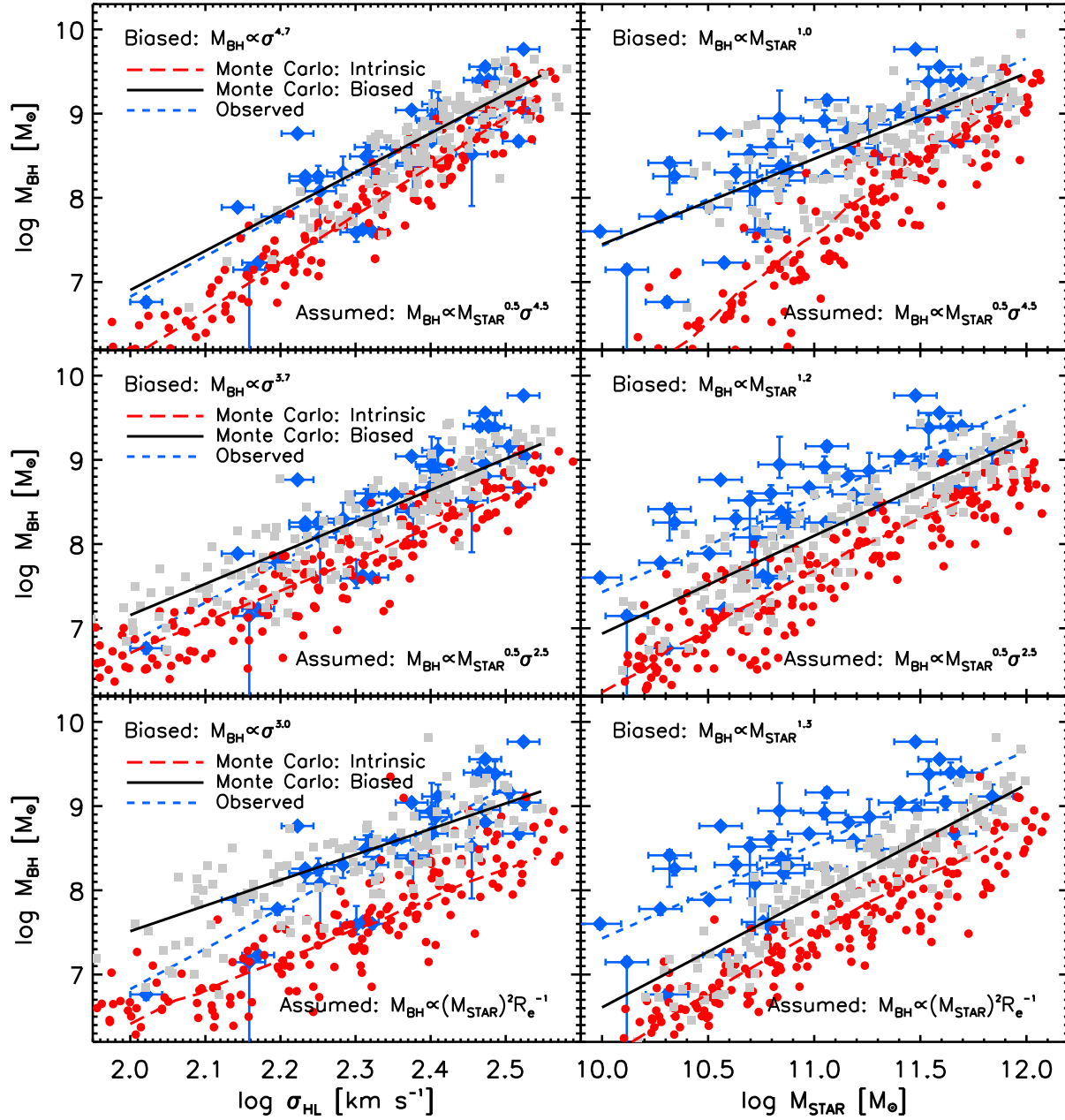


Figure 3. Black hole scaling relations: $M_{\text{bh}}-\sigma$ (left) and $M_{\text{bh}}-M_{\text{star}}$ (right), in Model I ($M_{\text{bh}} \propto M_{\text{star}}^{0.5} \sigma^{4.5}$, top), Model II ($M_{\text{bh}} \propto M_{\text{star}}^{0.5} \sigma^{2.5}$, middle), and Model III ($M_{\text{bh}} \propto M_{\text{star}}^2/R_e$, bottom) in the same format as the previous figure. Red circles and grey squares show a random subsample of 200 objects from the full and selection biased subsamples, respectively. Red long-dashed and black solid curves show the associated mean values of M_{bh} as σ and M_{star} vary. Resolving the black hole sphere of influence biases the observed relations so that they lie significantly above the intrinsic ones; they overestimate M_{bh} by factors of $3\times$ or more. Blue symbols with error bars show the Savorgnan et al. (2016) dataset which is only really matched by the (selection biased) Model I.

σ). Correlations with the variable on which the selection was made will be unbiased, and, since the correlation shown is at fixed M_{star} , the r_{infl} selection does not bias the σ - M_{star} relation in the middle panel very much. However, in Model I, $r_{\text{infl}} \propto M_{\text{star}}^{0.5} \sigma^{2.5}$ is nearly a function of σ only, so requiring $\theta_{\text{infl}} \geq \theta_{\text{crit}}$ will tend to select large σ , which is what we see in the left hand panel. In contrast, $r_{\text{infl}} \propto (M_{\text{star}}^2/R_e)/\sigma^2$ in Model III, so $\theta_{\text{infl}} \geq \theta_{\text{crit}}$ tends to select small σ in the right hand panel.

Comparison with the blue symbols in the top panels shows that Model I is remarkably similar to the data, whereas Models II

and III are not. The discrepancy between the σ - M_{star} relation in the selection-biased sample and the data (i.e., the Savorgnan et al. 2016 E+S0s) is most pronounced in Model III, because it has no σ factor in M_{bh} to cancel the σ^2 factor in the definition of r_{infl} , so the selection biased sample is composed of objects with smaller σ (rather than larger) for their M_{star} .

For completeness, the bottom panels of Figure 2 show a similar analysis of the R_e - M_{star} relation. Model II is nearly unbiased by the selection effect for the same reason as before; and while there is a small bias (to slightly smaller R_e) in models I and III, it

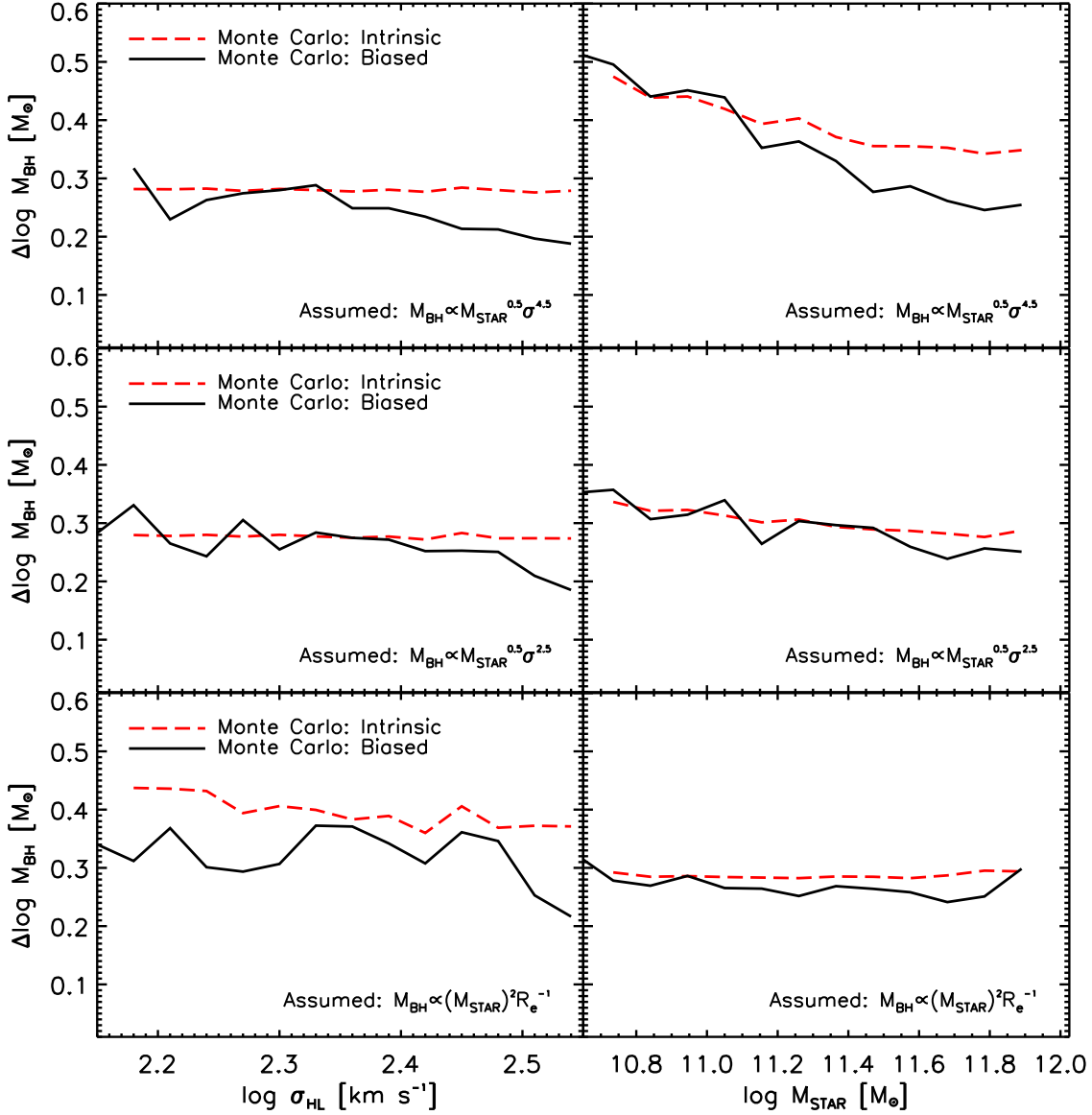


Figure 4. Scatter around the mean relations for the mock catalogues shown in Figure 3. Long-dashed red lines mark the intrinsic scatter around the mean relations; solid black lines show the scatter in the selection-biased subsamples. The decreasing scatter in the $M_{\text{bh}}-M_{\text{star}}$ relation for Model I (upper right), which is amplified in the selection biased sample, is a direct consequence of the fact that the scatter around the mean $\sigma-M_{\text{star}}$ relation decreases at large M_{star} (Figure 1).

is much smaller than for $\sigma-M_{\text{star}}$.⁴ All the models are in reasonable agreement with the Savorgnan et al. (2016) data.

4.3 Selection-biased M_{bh} scaling relations

Having shown that the selection biased samples are similar to the data – with Model I faring better than the other two models for $\sigma-M_{\text{star}}$ (in general, the dependence on velocity dispersion, labelled by the slope β , must be large to explain the observed offset in the $\sigma-M_{\text{star}}$ relation) – and that the selection biased Model I sample is

⁴ The slight bias can be understood in terms of the virial theorem: at fixed M_{star} , large σ means smaller R_e , and we know that the selection effect in Model I favours large σ . The bias appears small because the intrinsic R_e-M_{star} relation is tighter, i.e. has less scatter, than the $\sigma-M_{\text{star}}$ relation.

biased compared to the intrinsic $\sigma-M_{\text{star}}$ relation – we now turn to correlations with M_{bh} .

Figure 3 shows the $M_{\text{bh}}-\sigma$ (left) and $M_{\text{bh}}-M_{\text{star}}$ (right) relations in our Monte Carlo simulations based on Model I (top), Model II (middle), and Model III (bottom). All models predict biased scaling relations that have higher normalizations and in some cases flatter slopes than the intrinsic ones. This is the main reason why we chose lower normalization factors γ for all our Monte-Carlo models (cfr. Section 4.1). This bias becomes more pronounced as the input slope β or the input scatter increase (also see discussion of Figure 9). This is why the bias induces a stronger upwards boost in the $M_{\text{bh}}-M_{\text{star}}$ relation for Model I than Model II or III (right panels).

In addition, notice the curvature in the intrinsic $M_{\text{bh}}-M_{\text{star}}$ relation (long-dashed red lines in the panels on the right), which is most evident for Model I. Since Equation 4, which we used to

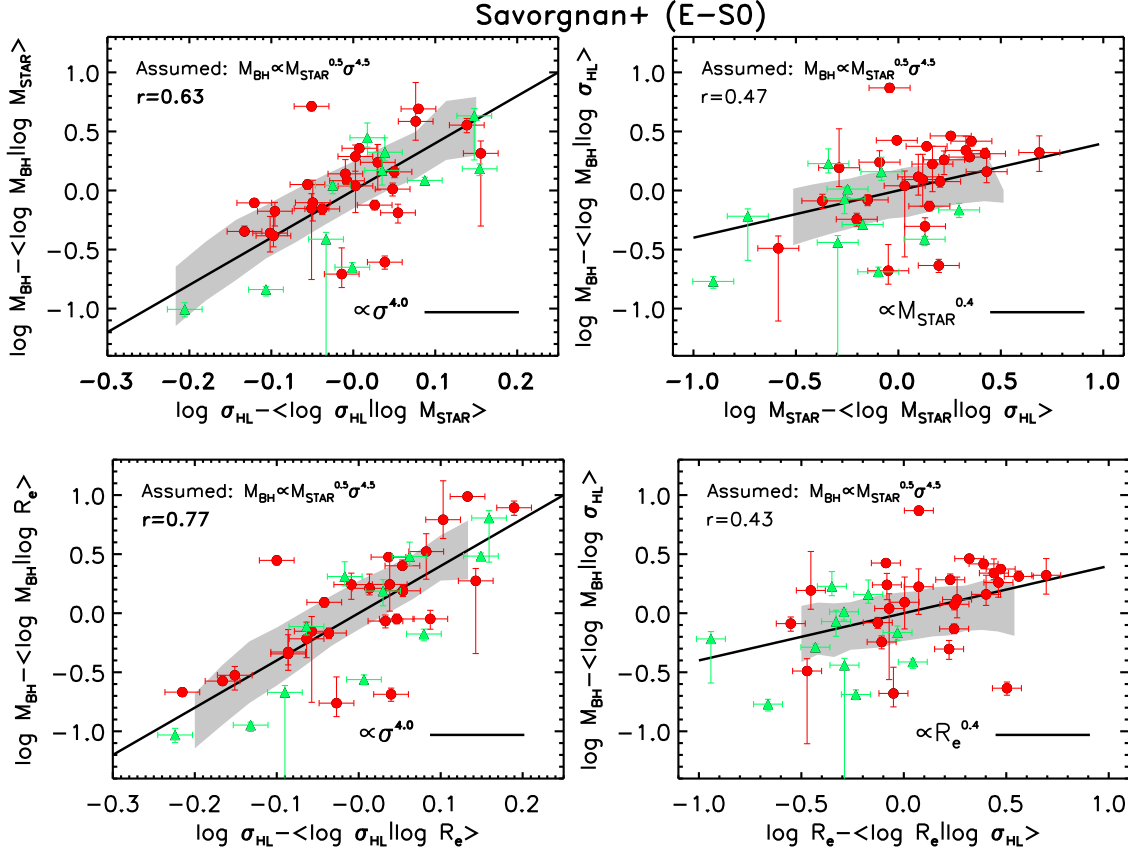


Figure 5. Correlations between residuals from the observed scaling relations, as indicated. Red circles and green triangles show E and S0 galaxies from the Savorgnan et al. (2016) E–S0 sample, while grey bands show the corresponding measurements in our (selection biased) Model I. The selection bias tends to reduce the slope of the $M_{\text{bh}}-\sigma$ relation (from $\beta = 4.5$ to ~ 4), so solid lines in panels on the left show a slope of 4. In the panels on the right, solid lines with a slope of 0.4 approximate the expected scalings with stellar mass or effective radius in the biased samples. Correlations with velocity dispersion appear to be stronger than those with the other two quantities, in good agreement with Model I.

generate M_{bh} , assumes pure power-law relations, this curvature is entirely a consequence of curvature in the σ – M_{star} relation (Figure 1). Curvature in the observed (selection biased) $M_{\text{bh}}-M_{\text{bulge}}$ relation has been reported by Graham & Scott (2013). Our analysis suggests that this curvature is due to galaxy formation physics, and need not imply anything fundamental about black hole formation or mergers (see also Fontanot et al. 2015). The intrinsic $M_{\text{bh}}-M_{\text{star}}$ relation in Model I can be approximated by

$$\log \frac{M_{\text{bh}}}{M_{\odot}} = 7.574 + 1.946 \log \left(\frac{M_{\text{star}}}{10^{11} M_{\odot}} \right) - 0.306 \times \left[\log \left(\frac{M_{\text{star}}}{10^{11} M_{\odot}} \right) \right]^2 - 0.011 \left[\log \left(\frac{M_{\text{star}}}{10^{11} M_{\odot}} \right) \right]^3, \quad (6)$$

while the intrinsic $M_{\text{bh}}-\sigma$ relation is

$$\log \frac{M_{\text{bh}}}{M_{\odot}} = 7.8 + 5.7 \log \left(\frac{\sigma_{\text{HL}}}{200 \text{ km s}^{-1}} \right). \quad (7)$$

The first reflects the curvature in the σ – M_{star} relation, and the second is consistent with the $M_{\text{star}}-\sigma$ relation having a linear scaling of the type $M_{\text{star}} \propto \sigma^{2.4}$, at least below $\sigma \lesssim 260 \text{ km s}^{-1}$. The Milky Way to date is the best resolved dynamical measurement of a central black hole with $M_{\text{bh}} \sim 4.3 \times 10^6 M_{\odot}$, $\sigma \sim 200 \text{ km s}^{-1}$ (Scott et al. 2013) and stellar mass of $\log M_{\text{star}} \sim 10.7$ (e.g., Licquia & Newman 2015, for a Chabrier IMF). It is also awkwardly renowned to be a strong outlier with respect to the observed scaling

relations especially with stellar mass (e.g., Marconi & Hunt 2003), but it is instead fully consistent with our intrinsic relations of Model I.

Having illustrated the bias in the mean relations, we now consider the scatter around the relations, computed in our mocks as the 1σ dispersion around the mean. The six panels in Figure 4 are for the same relations shown in Figure 3: the long-dashed, red lines show the scatter in the full sample (i.e., the scatter around the long-dashed red lines in Figure 3), and the black solid lines show the scatter measured in the selection biased subsample (the scatter around the black lines in Figure 3). In all models, the scatter in the biased samples is comparable to, or as much as $\sim 30\%$ smaller than, the intrinsic scatter. Although the data are too sparse to allow a reliable determination of the scatter, they do show a tendency to decrease at large masses which is in qualitative agreement with our simulations.

It is sometimes argued that because the observed scatter around the $M_{\text{bh}}-M_{\text{star}}$ relation is of the same magnitude as that around the $M_{\text{bh}}-\sigma$ relation, especially in early-type, massive galaxies, it is plausible that the $M_{\text{bh}}-M_{\text{star}}$ relation is at least as, if not more, fundamental. However, the top panels show that this argument is flawed because in Model I velocity dispersion is more important than stellar mass: the scatter around the observed $M_{\text{bh}}-M_{\text{star}}$ relation seems comparable to the one on the left panel, especially at large masses, because of the selection effect. In addi-

tion, some groups have reported a tendency for the scatter to decrease at large masses in models characterized by repeated black hole-black hole mergers (e.g., Peng 2007; Jahnke & Macciò 2011; Hirschmann et al. 2010). Figure 4 suggests that such arguments should be treated with caution, as this trend, clearly observed in Model I (upper panels), entirely reflects the decrease in scatter in the velocity dispersion with increasing stellar mass (Figure 1) which the selection bias amplifies (solid line). Graham & Scott (2013) have addressed this point differently, by arguing that the low-mass end of the $M_{\text{bh}}-M_{\text{bulge}}$ diagram does not converge to a relation with a slope of unity, as required in the many-merger scenario.

4.4 Selection-biased black hole demographics

The selection effect has another important consequence. If one uses the observed $\sigma-M_{\text{star}}$ (or bulge mass) relation to translate between σ and M_{star} , then the observed $M_{\text{bh}}-\sigma$ relation predicts a factor of ~ 3 lower black hole masses than the observed $M_{\text{bh}}-M_{\text{star}}$ relation (Tundo et al. 2007; Bernardi et al. 2007; Graham et al. 2007). Accounting for the scatter around these relations does not resolve the discrepancy (Tundo et al. 2007). The selection-biased relations (black lines in Figure 1) in our Monte Carlo simulations result in a similar discrepancy. For example, in Model I, $\log(M_{\text{star}}/M_{\odot}) = 11$ would predict a black hole mass of $\log(M_{\text{bh}}/M_{\odot}) \sim 8.4$ (upper right). Figure 1 (right panels) shows that $\log(M_{\text{star}}/M_{\odot}) = 11$ corresponds to $\log(\sigma_{\text{HL}}/\text{km s}^{-1}) \sim 2.25$, for which the solid line in the upper left panel of Figure 3 suggests $\log(M_{\text{bh}}/M_{\odot}) \sim 7.9$. This discrepancy is somewhat smaller, but still present, in the other two models. Accounting for the scatter around these selection-biased relations does not resolve the discrepancy. These are selection effects: in all models the discrepancy is much smaller if one uses the intrinsic relations (long-dashed red curves), and it disappears entirely (by definition) if one accounts for the intrinsic scatter.

In this context, the results from the cosmological black hole model presented by Sijacki et al. (2015) and developed in the framework of the Illustris simulation (Vogelsberger et al. 2014) are informative. When normalized to the (biased) black hole mass-bulge stellar mass relation, their model systematically overproduces the $M_{\text{bh}}-\sigma$ relation by a factor of $\gtrsim 3$ at $\log(\sigma/\text{km s}^{-1}) \gtrsim 2.3$ (their Figure 6). Our work suggests this is a consequence of normalizing to a relation that has been biased by selection effects, rather than to the intrinsic relation.

4.5 Correlations between residuals

Studying correlations between the residuals from various scaling relations is an efficient way of determining if a variable is fundamental or not. For example, if M_{bh} is determined by σ alone (e.g., if $\alpha = 0$ in Model I) then residuals from correlations with σ should be uncorrelated. In this case, residuals from the $M_{\text{bh}}-$, $M_{\text{star}}-$, and $R_e-\sigma$ relations should not correlate with one another (e.g., Bernardi et al. 2005; Sheth & Bernardi 2012). In contrast, not only should residuals from the $M_{\text{bh}}-M_{\text{star}}$ relation correlate with residuals from the $\sigma-M_{\text{star}}$ relation, but the slope of this correlation between residuals should be the same as that of the $M_{\text{bh}}-\sigma$ relation itself; this is what indicates that σ controls the $M_{\text{bh}}-M_{\text{star}}$ correlation.

The grey bands in each panel of Figure 5 show residuals along the y -axis from the scaling relations measured in the selection biased subsamples of Model I. In this Model, residuals from the true

intrinsic correlations with σ (left panels) should correlate with a slope of $\beta \sim 4.5$, and those as a function of stellar mass (or effective radius) with a slope of $\alpha \sim 0.5$. This is indeed what the simulations show, though the selection bias tends to slightly flatten the slope of the $M_{\text{bh}}-\sigma$ relation (top left panel of Figure 3) from a slope of $\beta = 4.5$ to $\beta \sim 4$ and also the biased $\alpha \sim 0.3 - 0.4$. This flattening would be even more pronounced for higher values of the intrinsic β and/or scatter (see discussion of Figure 9).

The red circles (ellipticals) and green triangles (S0s) in the same Figure 5 show a similar analysis of the residuals from scaling relations in the observed E+S0 sample of Savorgnan et al. (2016). The slopes in all the panels on the left are $\beta \sim 4$. We quantify the strength of each correlation using the Pearson correlation coefficient r , which we report in the top left corner of each panel. These values show that the correlations on the right are weaker than those on the left, indicating that σ is the more important of each pair. This is important as it shows that the selection biased sample still correctly indicates that σ is more fundamental.

In each panel, the grey band defined by Model I is consistent with the correlation measured in the Savorgnan et al. (2016) sample. Figure 6 shows a similar analysis of Model II; the grey bands in the left hand panels show that the dependence on σ in this model is weaker than in the data.

Despite the small size of the dataset, we have attempted to quantify the uncertainties on the trends shown in the previous figures by using a bootstrapping technique. We randomly remove three sources from the Savorgnan et al. (2016) sample, measure the correlations and hence the residuals from the correlations, record the slope and scatter for the correlations between residuals, and repeat 100 times. For the Monte-Carlos, we instead generate 100 mock samples, each having 50 objects, for which we measure the slope and scatter of the correlations between residuals.

The mean slopes and standard deviations over the 100 realizations are reported in Table 1. The second, third, and fourth columns report the results of the bootstrapping on the data considering only E-S0, all galaxies, and all bulges, respectively, while the fifth/sixth, seventh, and eighth columns are the results of Model I (total and bulge stellar masses), Model II, and Model III, respectively. This shows that Model I-total stellar masses (column 5) provides slopes that are well consistent with those of the E-S0 Savorgnan et al. (2016) sample (column 2). However, the uncertainties on the slopes are relatively large, so even Model II, which tends to predict flatter slopes than what observed (Figure 6), is only discrepant at the $1 - 2\sigma$ level. Model III, the residuals of which are shown in Appendix B, appears to be more than 2σ discrepant, especially in the residuals of velocity dispersion at fixed stellar mass (first row).

A similar analysis of the residuals in the Saglia et al. (2016), McConnell & Ma (2013), Läsker et al. (2014), and Beifiori et al. (2012) samples is included in Appendix A, with the results of the statistical analysis reported in Table 2 (columns 3, 4, 5, and 6, respectively), compared to the Savorgnan et al. (2016) sample (column 2) and the predictions of Model I (column 7). For all samples in Table 2 we restrict to E-S0 with total stellar masses and effective radii, except for the Saglia et al. (2016) dataset, for which only bulge masses and radii are available (for this sample we also include non-barred spirals). Mean slopes and uncertainties are again computed from 100 bootstrap iterations in which 3 sources were removed at a time, except for the smaller Beifiori et al. (2012) sample, for which we only removed a single object at a time. These other samples show the same trends we found in the Savorgnan et al. (2016) sample. If anything, the de-

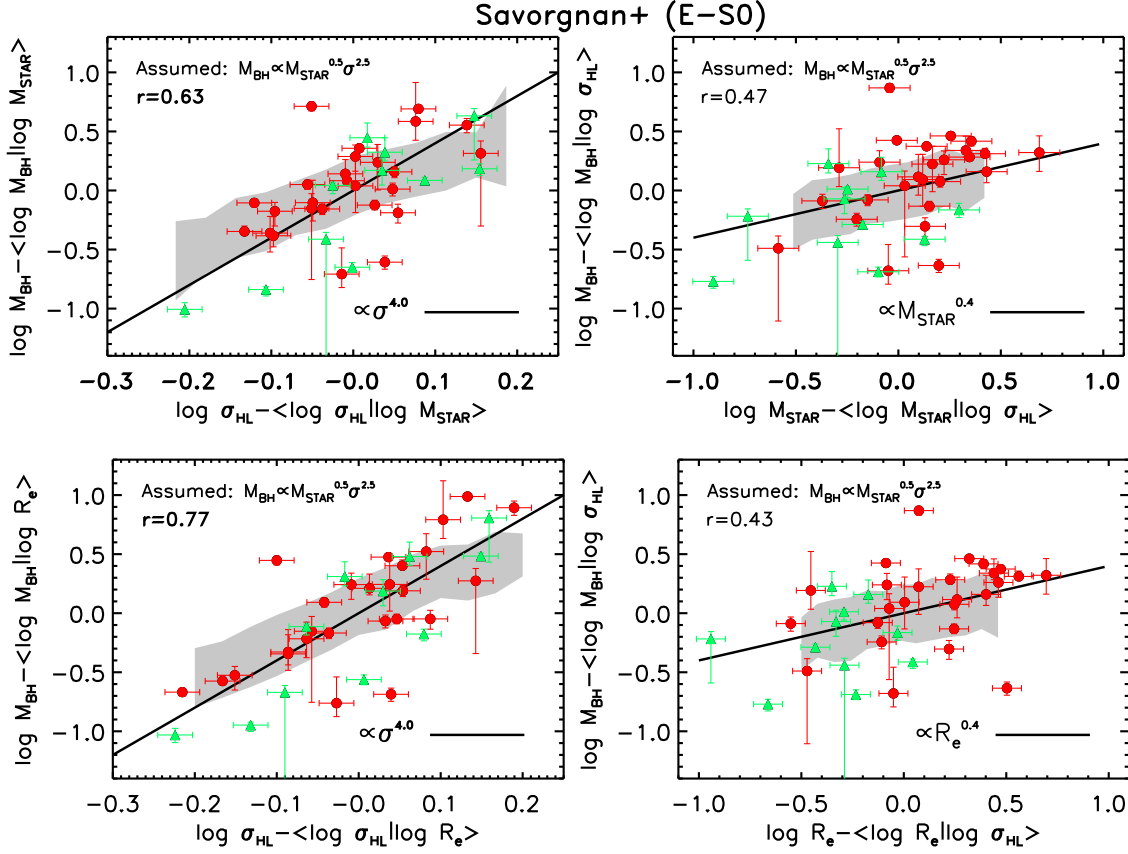


Figure 6. Same as Figure 5, but with grey bands now showing our (selection biased) Model II. The dependence on σ (left hand panels) is weaker than in the data.

Table 1. Mean slope and its uncertainty for the correlation between residuals named in the first column. The compact notation in the first column has the meaning $\Delta(X|Y) = \log X - \langle \log X | \log Y \rangle$. The second, third, and fourth columns are for the $E - S0$ s, all galaxies, and all bulges from Savorgnan et al. (2016). The fifth, sixth, seventh, and eighth columns are the corresponding results from the Monte Carlo simulations of Model I (total and bulge stellar masses), Model II, and Model III. Model I tends to be in better agreement with the data, though uncertainties are still substantial (see text for details).

Residual	E-S0	All	All bulges	Model I	Model I (bulges)	Model II	Model III
(1)	(2)	(3)	(4)	(5)	(6)	(7)	(8)
$\Delta(M_{bh} M_{star})$ vs $\Delta(\sigma M_{star})$	3.24 ± 0.64	4.42 ± 0.58	3.60 ± 0.51	3.68 ± 1.30	3.97 ± 1.40	2.47 ± 0.80	0.44 ± 1.02
$\Delta(M_{bh} R_e)$ vs $\Delta(\sigma R_e)$	3.94 ± 0.47	4.70 ± 0.43	3.86 ± 0.43	4.45 ± 1.00	4.99 ± 1.05	3.18 ± 0.53	2.73 ± 0.83
$\Delta(M_{bh} \sigma)$ vs $\Delta(M_{star} \sigma)$	0.54 ± 0.14	0.34 ± 0.16	0.42 ± 0.09	0.35 ± 0.24	0.34 ± 0.25	0.47 ± 0.24	1.22 ± 0.44
$\Delta(M_{bh} \sigma)$ vs $\Delta(R_e \sigma)$	0.45 ± 0.14	0.31 ± 0.15	0.41 ± 0.09	0.54 ± 0.32	0.34 ± 0.24	0.38 ± 0.26	0.23 ± 0.53

Table 2. Same as Table 1, but now the second, third, fourth, fifth, and sixth columns are from the $E + S0$ s of Savorgnan et al. (2016), Saglia et al. (2016), McConnell & Ma (2013), Läscher et al. (2014), and Beifiori et al. (2012). The other samples are in good agreement with the Savorgnan et al. (2016) sample and with Model I (seventh column), suggesting, if anything, an even weaker dependence on stellar mass.

Residual	Savorgnan+	Saglia+	McConnell&Ma	Läscher+	Beifiori+	Model I
(1)	(2)	(3)	(4)	(5)	(6)	(7)
$\Delta(M_{bh} M_{star})$ vs $\Delta(\sigma M_{star})$	3.24 ± 0.64	3.47 ± 0.65	3.60 ± 0.94	4.39 ± 0.95	4.36 ± 0.81	3.68 ± 1.30
$\Delta(M_{bh} R_e)$ vs $\Delta(\sigma R_e)$	3.94 ± 0.47	3.72 ± 0.52	4.16 ± 0.71	4.63 ± 0.89	3.95 ± 0.62	4.45 ± 1.00
$\Delta(M_{bh} \sigma)$ vs $\Delta(M_{star} \sigma)$	0.54 ± 0.14	0.23 ± 0.13	0.39 ± 0.23	0.33 ± 0.19	0.09 ± 0.94	0.35 ± 0.24
$\Delta(M_{bh} \sigma)$ vs $\Delta(R_e \sigma)$	0.45 ± 0.14	0.26 ± 0.12	0.39 ± 0.22	0.39 ± 0.24	0.05 ± 0.28	0.54 ± 0.32

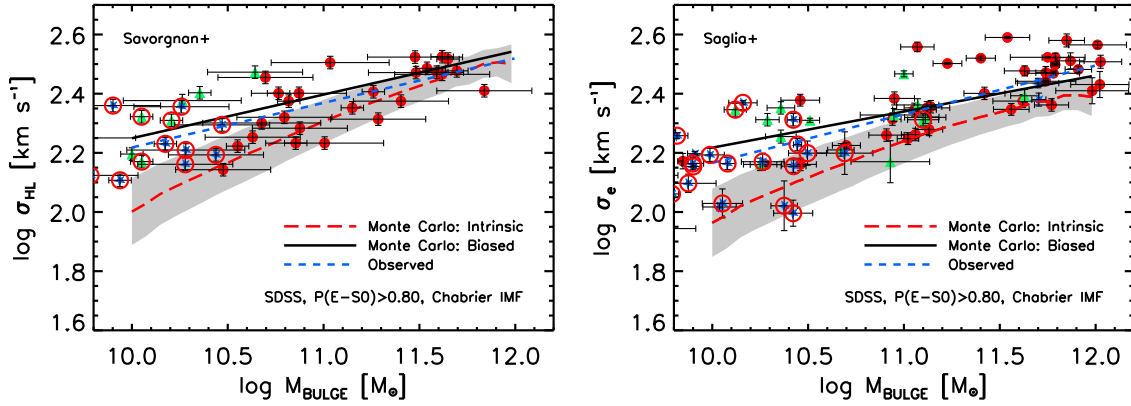


Figure 7. Left: Same as top right panel of Figure 1 but with M_{bulge} rather than total M_{star} for the sample of Savorgnan et al. (2016). Right: Same as left panel but for the sample of Saglia et al. (2016), for which we have used σ_e as σ_{HL} is not available. We also include results of the Model I Monte Carlos when using only bulge stellar masses. Filled red circles, green triangles, and blue stars in both panels correspond, respectively, to ellipticals, S0, and the bulges of spirals. Open red circles mark the galaxies with bars. The predicted biased relations (black, solid lines) agree well with those observed (blue, dashed lines).

pendence on σ is stronger, and that on M_{star} or R_e is weaker, so that Model I fares better than the others.

4.6 The impact of spirals and bulge-to-total decompositions

In the previous section we noted that the residuals around the black hole-galaxy scaling relations suggest that velocity dispersion is the most important property of a galaxy with regards to the black hole at its centre. That analysis was based on a sample of early-type galaxies. In this section we include the spirals from the Savorgnan et al. (2016) with “secure” black hole mass measurements as reported in Kormendy & Ho (2013). As for the early-types, velocity dispersions for these galaxies are taken from the Hyperleda data base and total half-light radii are derived as explained in Section 2.

In the context of including spirals, however, it is possible that the bulge mass is more relevant than the total. We noted in Section 2 that M_{bulge} is significantly more difficult to estimate reliably (e.g. Meert et al. 2013). Nevertheless, Meert et al. (2015) provide B/T decompositions for their Sérsic-Exponential reductions, which we have used to estimate M_{bulge} in the SDSS. Savorgnan et al. (2016) also considered detailed galaxy decompositions that take into account spheroid, discs, spiral arms, bars, rings, halo, extended or unresolved nuclear source and partially depleted core, and checked for consistency with galaxy kinematics (e.g., Arnold et al. 2014). So, we have used bulge stellar masses to see how the offset in the top right panel of Figure 1 changes when we replace $M_{\text{star}} \rightarrow M_{\text{bulge}}$. We continue to restrict the analysis to E-S0 SDSS galaxies, as determining the central velocity dispersion of spirals from the SDSS spectra (which are not spatially resolved) is not possible. Adopting the E-S0 bulge sample as representative of the full galaxy population between $10^{10} < M_{\text{star}}/M_{\odot} < 10^{12}$ is a safe assumption given that the bulges of spirals have structural properties that follow the scaling relations of the bulges of early-type galaxies quite well (e.g., Bernardi et al. 2014).

The left panel of Figure 7 shows the Savorgnan et al. (2016) data with spirals included (blue stars), but using M_{bulge} rather than total masses. It shows that there is a clear offset from the σ - M_{bulge} relation of the SDSS, qualitatively like that seen in Figure 1. The significantly larger error bars reflect the larger uncertainties in estimating M_{bulge} . Later-type galaxies show the largest offsets, in

agreement with Graham (2008). Also note that the Meert et al. (2015) reductions have a slight systematic tendency to set $B/T \approx 0.9$ even when $B/T = 1$ (see Figure 9 of Meert et al. 2013). Therefore, at large M_{bulge} where we expect to have $B/T \rightarrow 1$, the SDSS relation is shifted slightly more to the left than it should be. Removing this systematic would slightly increase the offset between the SDSS and the Savorgnan et al. (2016) sample.

The right panel of Figure 7 compares the SDSS σ - M_{bulge} relation with the bulge masses and velocity dispersions in the sample of Saglia et al. (2016). The offset between the two data sets here is slightly more pronounced than it was for the Savorgnan et al. (2016) data (on the left). Note that the mass-to-light M/L ratios adopted by Saglia et al. (2016) are dynamical ones: they are not derived from spectral analysis. Saglia et al. (2016) argue that their M/L are broadly consistent with those obtained assuming a Kroupa (Kroupa 2001) IMF which, if anything, should yield systematically larger stellar masses at fixed velocity dispersion than those obtained from a Chabrier IMF as in SDSS (e.g., Bernardi et al. 2010). We also include in Figure 7 the results of our Monte Carlo simulations with Model I in which we replace M_{star} with M_{bulge} . It can be seen that the predicted, biased σ - M_{bulge} relation from Model I (solid black lines) reproduces the measured slopes and normalizations in both samples (dashed blue lines).

In both panels of Figure 7, red circles identify disc galaxies with a bar. These tend to have similar σ to barless galaxies of the same M_{bulge} . Thus, as we noted when discussing Figure 2, the selection bias does not seem to be affected strongly by the presence of a bar.

In view of the similarities between Figure 1 and Figure 2, it should not be surprising that the corresponding M_{bh} - σ and M_{bh} - M_{bulge} relations are also biased by the selection effect. Therefore, rather than showing this explicitly, we consider the correlations between residuals from these scaling relations defined using bulge luminosities and effective radii. Figure 8 – the analogue of Figure 5 – shows results for the Savorgnan et al. (2016) sample. It is clear that spirals (blue stars) follow similar relations to those defined by earlier-type galaxies (red circles and green triangles). The slopes, reported in Table 1 (column 4), match those from the E-S0 sample well (column 2), though the dependence on σ is stronger and that on M_{bulge} weaker. For completeness, column 3, labeled “All”, reports the results of using the total M_{star} rather than M_{bulge} even for spirals. The grey bands in the various panels show (selection

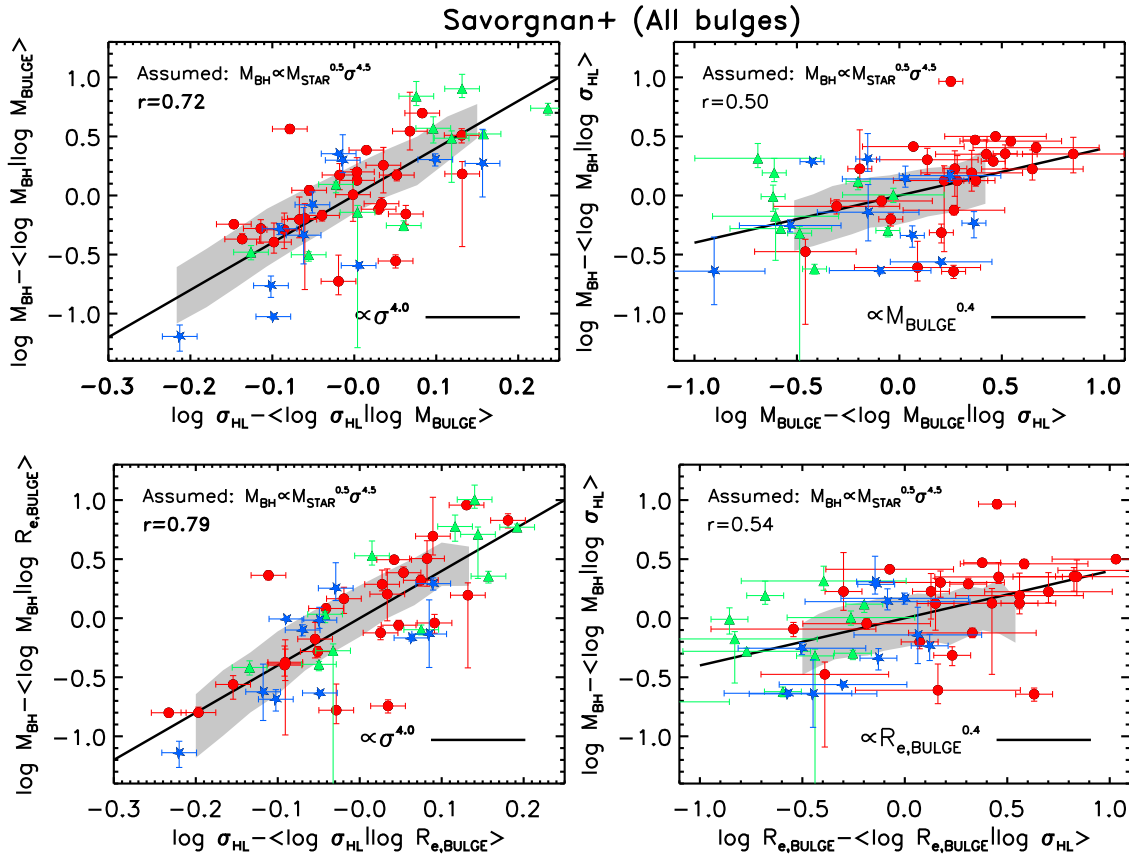


Figure 8. Same as Figure 5 with data from the Savorgnan et al. (2016) sample of bulge stellar masses and effective radii. The red circles, green triangles, and blue stars refer to the bulges of ellipticals, S0s, and spirals, respectively. The grey bands show the predictions from our (selection biased) Model I with bulge stellar masses and effective radii. Spirals continue to show residuals similar to those of early-type galaxies, with the residuals in velocity dispersion still being much stronger than with other galactic properties, in agreement with Model I.

biased) Model I when bulge stellar masses and effective radii are used (slopes reported in column 6 of Table 1); these are in good agreement with the data.

In summary: Bulges of spirals follow similar relations to those defined by earlier-type galaxies (red circles and green triangles). They too show a stronger dependence on velocity dispersion (left panels) than other properties (right). Moreover, the addition of spirals increases the baseline over which the relations on the left can be measured; this tightens the correlations with σ and weakens those with the other properties. This justifies our earlier claim that our results are not much affected by the use of stellar or bulge mass, and also further supports the scenario in which spirals, or better their bulges, are correlated with their central black holes via a steep $M_{\text{bh}}-\sigma$ relation, similarly to early-type galaxies. Evidently, σ is much more important than either total or bulge luminosity and/or size.

4.7 Dependence on strength of correlation with σ

Comparison of our selection-biased Monte Carlo simulations with the observations suggests that σ plays an important, if not fundamental, role in determining M_{bh} . However, we have not yet explored the range of acceptable values of the free parameters in our Model I. Figure 9 shows the result of setting $M_{\text{bh}} \propto M_{\text{bulge}}^{0.5} \sigma^\beta$ and producing Monte Carlo simulations for a range of values of the slope β , and rms scatter δ (blue short dashed, cyan long dashed, and

red dot-dashed as labelled). As mentioned in Section 4.1, a larger δ results in a larger selection bias, so a lower input normalization is required to reproduce the same set of observational data. Therefore, we reduce γ when δ is large (black, dotted lines in the upper, right panel). In the specific, when $\delta = 0.25$ dex we set $\gamma = 7.7$, as in Equation 4, while $\gamma = 8.0$ and $\gamma = 6.6$ for $\delta = 0.1, 0.5$ dex, respectively. Also, because of how our simulations are set-up, our δ includes a potential contribution from measurement errors on the value of M_{bh} . So, while they may not be the truly intrinsic values, comparing them with data, to which measurement error has contributed, is meaningful.

The top panels show how the slope and zero-point of the selection-biased $M_{\text{bh}}-\sigma$ relation we measure in our Monte Carlo simulations depends on the intrinsic slope and scatter; the middle panels show a similar study of the selection biased $M_{\text{bh}}-M_{\text{bulge}}$ relation; the bottom panels compare with the selection-biased $\sigma-M_{\text{bulge}}$ relation (left panel of Figure 7). Dotted lines in the top two panels show the input values; these show that the bias increases – slope decreases and zero-point increases – as the rms scatter increases. In all cases, the dashed, blue lines and grey bands show the range of slopes and zero-points which the bulge sample of Savorgnan et al. (2016) allow. Requiring the models to match these bands in all six panels shows that the intrinsic relation should have $\gamma \sim 7.7$, $\beta \sim 5$ and total scatter $\delta \sim 0.25$ dex. While models with small values of the input (total) scatter, e.g. $\delta = 0.1$, may also be acceptable, they tend to be less realistic in view of the non-

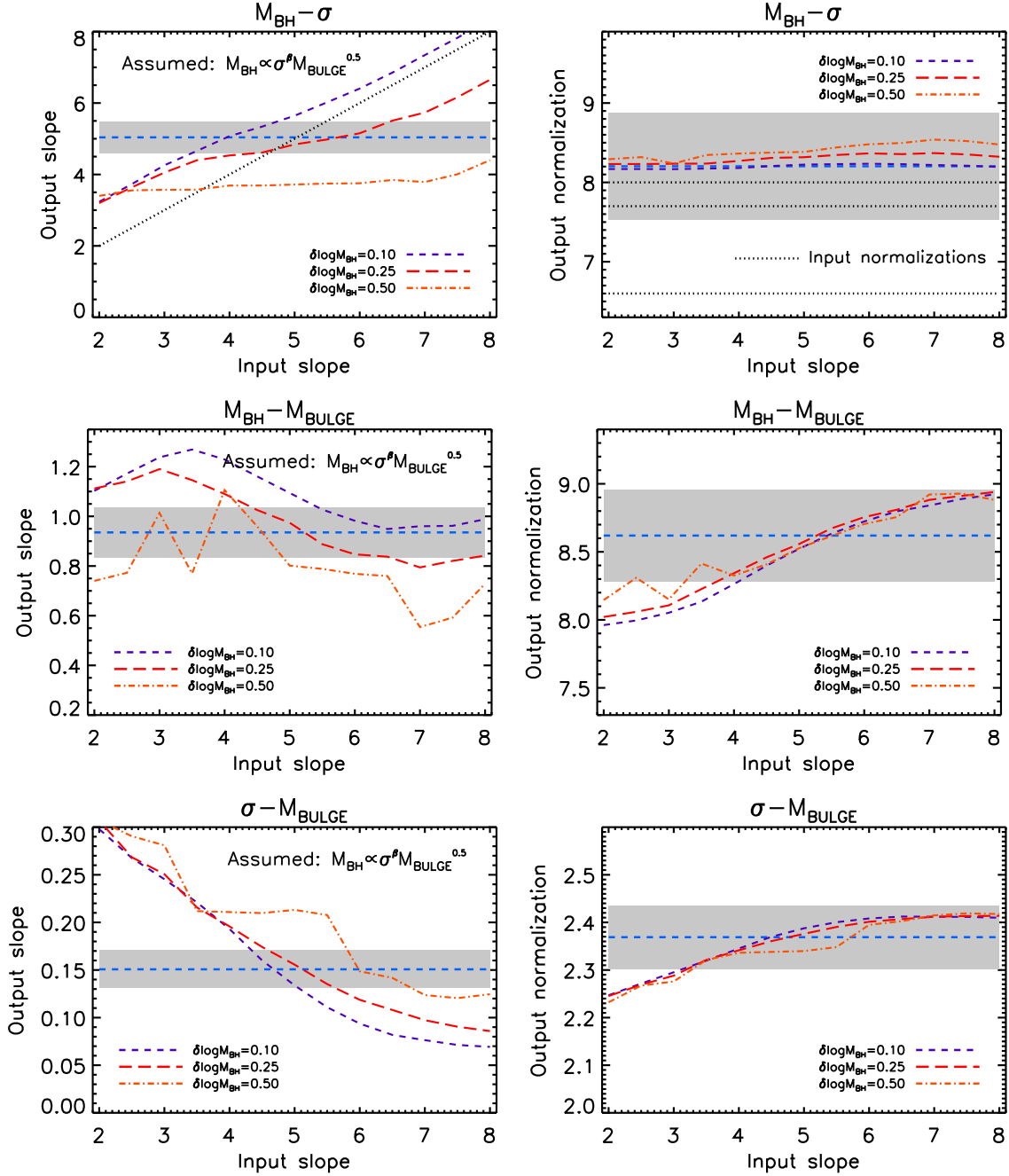


Figure 9. Dependence of the selection-biased slope (left) and normalization (right) on the intrinsic slope β and scatter δ for our Model I ($M_{\text{bh}} \propto M_{\text{star}}^{0.5} \sigma^\beta$). Upper, middle, and lower panels show results for the selection-biased $M_{\text{bh}} - \sigma$, $M_{\text{bh}} - M_{\text{star}}$, and $\sigma - M_{\text{star}}$ relations. Short-dashed, long-dashed and dot-dashed lines in each panel are for different values for the intrinsic scatter, as labelled. The dotted black lines in the right upper panel mark the three different normalizations chosen for each different value of the scatter; the lower normalizations correspond to higher values of δ . The dotted black line in the upper left panel shows a simple one-to-one relation to guide the eye. The solid lines and grey regions mark the mean and dispersions in the E+S0 sample of Savorgnan et al. (2016). Models with substantial scatter (> 0.3 dex) and/or input slopes much flatter or steeper than $\beta \sim 5$ are disfavoured by the data.

negligible observational uncertainties in the dynamical M_{bh} estimates (e.g., Ferrarese & Ford 2005). Allowing for 0.2 dex of M_{bh} measurement uncertainties, an observed scatter of $\delta \sim 0.25$ dex, allows for intrinsic scatter of ~ 0.15 dex. Our results are in line with the Monte Carlo simulations by Morabito & Dai (2012) and Gültekin et al. (2009) who both independently noticed that when the sphere of influence of the black hole is taken into account, the intrinsic slope in the $M_{\text{bh}} - \sigma$ relation becomes steeper $\beta \gtrsim 4 - 5$,

and the normalization lower than what actually measured by a factor of $\gtrsim 2$. A more quantitative comparison with their results is hindered by the fact that their simulations differ substantially from ours, which are based on a realistic large distribution of local, unbiased galaxies with proper measurements of stellar masses, velocity dispersion and effective radii.

Section 5 discusses the implications of the values $\gamma \sim 7.7$,

$\beta \sim 5$ and $\delta \lesssim 0.3$ dex for our understanding of the co-evolution of black holes and their host galaxies.

4.8 Calibration of other M_{bh} proxies

Without significant improvements in technology, it is difficult to measure dynamical masses at smaller M_{bh} locally, or at all at significant redshift. The alternative is to look for other observational signatures of M_{bh} which do not require that r_{infl} be resolved. Active galaxies are interesting in this respect since they can be observed both locally and at greater distances, so the same observational proxy for M_{bh} can be used over a wide range of redshift. The key step in this process is to calibrate these proxies using the dynamical mass estimates we have been discussing so far.

Recently Reines & Volonteri (2015) have compiled a sample of 262 broad-line AGN at $z < 0.055$ which roughly overlaps in volume with the dynamical mass black hole samples we have been discussing so far. Their “virial” M_{bh} estimates depend on a constant of proportionality $f_{\text{vir}} \approx 4.3$, whose value was calibrated by matching to a $M_{\text{bh}}-\sigma$ relation which is like that of the selection biased sample of Savorgnan et al. (2016). With this calibration, they find that their AGN sample has $\log(M_{\text{bh}}/M_{\odot}) = 7.45 + 1.05 \log(M_{\text{star}}/10^{11} M_{\odot})$. These M_{bh} values are substantially smaller than those for which dynamical M_{bh} measurements are available; the local (typically inactive) early-types have $\log M_{\text{bh}} = 8.9 + 1.23 \log(M_{\text{star}}/10^{11} M_{\odot})$. Is physics responsible for this factor of ~ 50 discrepancy, or are selection effects also playing a role here?

Regarding selection effects in this context, Graham et al. (2011) have argued that $f_{\text{vir}} \approx 2.8$ may be a more appropriate choice. Our own analysis suggests that, because of selection effects, the M_{bh} values in the AGN sample should be reduced by a much larger factor, $\gtrsim 3$, making $f_{\text{vir}} \approx 1$. In either case, reducing f_{vir} would exacerbate rather than reduce the apparent difference with the local $M_{\text{bh}}-M_{\text{star}}$ relation. However, this is not the full story. Recall that the selection bias is much more dramatic for $M_{\text{bh}}-M_{\text{star}}$ than for $M_{\text{bh}}-\sigma$ (top panels of Figure 3). So, it is possible that the AGN samples are probing lower masses where the $M_{\text{bh}}-M_{\text{star}}$ bias is particularly severe.

To illustrate, the blue squares in Figure 10 show the data of Reines & Volonteri (2015), with their M_{bh} values lowered by the (factor of three on average) difference between the intrinsic and selection biased Monte Carlo samples in Model I (top left panel of Figure 3). The blue dashed line – which lies substantially above the AGN sample – shows the selection biased $M_{\text{bh}}-M_{\text{star}}$ relation from the top right panel of Figure 3. The corresponding intrinsic $M_{\text{bh}}-M_{\text{star}}$ relation is shown by the red circles. The agreement between this intrinsic relation and the AGN sample is striking, particularly at $\log(M_{\text{star}}/M_{\odot}) \sim 10.5$, where the bulk of the AGN data lie.

Some of the remaining difference is a consequence of reporting results in terms of M_{star} rather than M_{bulge} , as it is likely that the relevant comparison is with M_{bulge} (see, e.g., Graham & Scott 2015). Whereas $M_{\text{star}} \approx M_{\text{bulge}}$ for the early-types with dynamical M_{bh} measurements, $M_{\text{bulge}} < M_{\text{star}}$ for the AGN sample. This would shift the blue squares to smaller M_{star} (i.e. to the left in Figure 10), further improving the match with the red circles (the unbiased Model I relation). This agreement means that essentially all the offset between these AGN data and current local dynamical mass black hole samples is a selection effect, and that $f_{\text{vir}} \approx 1$.

More recently, Läscher et al. (2016) analyzed nine megamaser disc galaxies with an average stellar mass of $M_{\text{star}} \sim 10^{11} M_{\odot}$ and

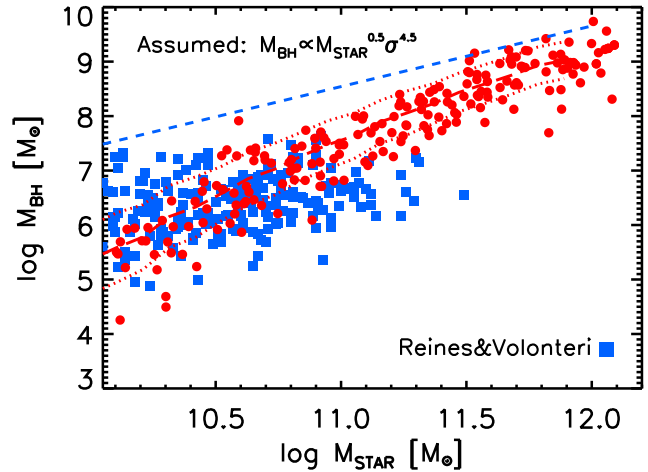


Figure 10. The $M_{\text{bh}}-M_{\text{star}}$ relation for the $z < 0.055$ broad line AGN sample of Reines & Volonteri (2015) (blue squares), shifted downwards by a factor of ~ 3 as described in the text (i.e., $f_{\text{vir}} \approx 1$); the intrinsic relation for our Model I (red circles); and the corresponding selection biased relation in Model I (dashed blue line).

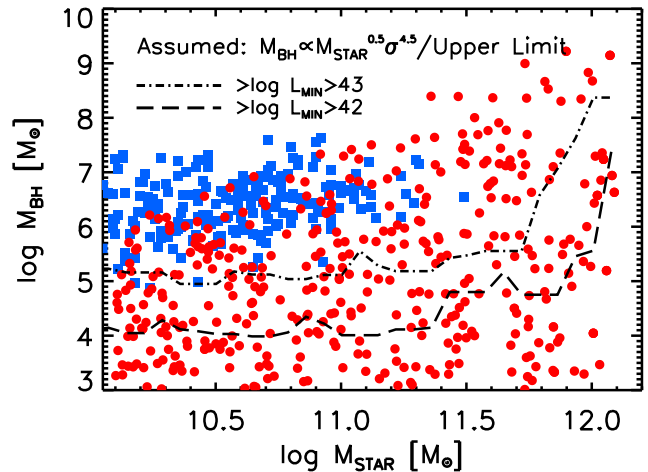


Figure 11. Predicted $M_{\text{bh}}-M_{\text{star}}$ relation for a model in which the scaling relation implied by Model I only represents an upper limit to the intrinsic distribution of black hole masses at fixed velocity dispersion (red circles). Dot-dashed and long-dashed lines show the smallest observable M_{bh} if the AGN is shining with the bolometric luminosity as labelled; the lower (long dashed) line is the luminosity cut imposed by Reines & Volonteri (2015), whose data are shown by the blue squares. The red circles which lie above this line show that, if the upper-limit model were correct, then many low mass black holes should have been detected. Since there are no blue squares at these low masses, the data rule out this model.

an average black hole mass of $M_{\text{bh}} \sim 10^7 M_{\odot}$. They report an offset of $\delta \log M_{\text{bh}}/M_{\odot} = -0.8 \pm 0.2$ with respect to the Läscher et al. (2014) best-fit $M_{\text{bh}}-M_{\text{star}}$ relation for inactive galaxies, which is consistent with the mean difference between our observed and intrinsic relations in Model I (Figure 3). Similarly, Ho & Kim (2014, see also Ho & Kim 2016), compared reverberation-mapped AGNs with measured bulge stellar velocity dispersions against the $M_{\text{bh}}-\sigma$ relation of inactive galaxies, finding a mean offset lower by $\delta \log M_{\text{bh}}/M_{\odot} = -0.79$ dex (see their Figure 2). The discussion above shows why we believe the discrepancy between the normalizations of the black hole scaling relations of active and

dynamically-based samples is in large part a selection effect in the latter.

4.9 On why we support the intrinsic black hole-galaxy scaling relation as a ridge

We complete this section by discussing the possibility put forward by Batcheldor (2010) that the intrinsic black hole-galaxy scaling relation is not a relatively narrow ridge, but that the observed relation represents the upper limit of a much broader, almost uniform, distribution of $\log M_{\text{bh}}$ at fixed σ . Ford et al. (1998) had already argued that the lack of objects with small M_{bh} and large σ means this is unlikely to be correct. Gültekin et al. (2011) added that if it were correct, there should be many more upper limits (i.e., non-detections, because $r_{\text{inf}} \ll 0.1''$ for most objects) in the literature than detections – but this is not observed.

To address this directly, we performed the same set of simulations as for Model I – varying the input slope, normalization and scatter of the “upper envelope” Model I relation (Equation 4) – and obtained results qualitatively similar to those reported in Figure 9. However, we believe that the relevant question is: Does the intrinsic distribution of M_{bh} extend to much smaller values than our Monte Carlo simulations have assumed?

Since even local dynamical M_{bh} samples cannot probe small M_{bh} , we again turn to the AGN sample of Reines & Volonteri (2015). As Figure 10 shows, this sample clearly has many small M_{bh} at small M_{star} but not at large M_{star} . (A rather tight correlation between low-mass active black holes and their hosts’ spheroidal stellar masses was also recently inferred by Graham & Scott 2015 by combining a number of independent data sets collected from the literature.) The blue squares in Figure 11 show this sample again. The red circles show the expected distribution if Batcheldor (2010) were correct; we assumed the intrinsic distribution was uniform in $\log M_{\text{bh}}$ from an upper envelope defined by the observed $M_{\text{bh}}-\sigma$ relation down to $10^3 M_{\odot}$, though our conclusions do not depend on the exact value. This shows clearly that the upper envelope model is not consistent with the local AGN sample. Had we not shifted the AGN samples downwards by a factor of three, the discrepancy with the red symbols would have been even more dramatic.

We have also carried out additional tests to probe the impact of flux limit effects on the observed distributions of Reines & Volonteri (2015). We assigned broad, Schechter-type Eddington ratio distributions to our mock black holes in line with empirical estimates (e.g., Shankar et al. 2013b; Schulze et al. 2015, and references therein). Long-dashed and dot-dashed lines in Figure 11 show the limiting active black hole mass that is still detectable above a bolometric luminosity of $L_{\text{bol}} = 10^{42} \text{ erg s}^{-1}$ and $L_{\text{bol}} = 10^{43} \text{ erg s}^{-1}$. It is clear that whatever the chosen input duty cycle of active black holes, at the minimum luminosity of $L_{\text{bol}} = 10^{42} \text{ erg s}^{-1}$ probed by Reines & Volonteri (2015), the detectable limit extends between one and two orders of magnitude below the data. We conclude that a very broad distribution of local black holes down to very low masses, even at large σ or M_{star} , is not favoured by current data on local active galaxies (see further discussion in Section 5).

5 DISCUSSION

5.1 Direct implications of the bias in the observed scaling relations between black holes and galaxies

We have confirmed previous findings that all local galaxies with dynamical black hole mass estimates are a biased subset of all galaxies and this indicates that black hole scaling relations currently in the literature are biased (Bernardi et al. 2007). Comparison of the selection-biased scaling relations in our Monte-Carlo simulations with observations, along with analysis of the residuals, strongly suggest that the $M_{\text{bh}}-\sigma$ relation is fundamental, with a possible additional, relatively weak dependence on stellar (bulge) mass. In particular, our analysis suggests that the observed $M_{\text{bh}}-M_{\text{star}}$ relation, and as a consequence correlations with any other photometric property such as Sérsic index (e.g., Graham & Driver 2007a), are all highly biased. The intrinsic correlation between black hole mass and host galaxy stellar mass (total or bulge) is, according to our study, mostly a consequence of the $M_{\text{bh}}-\sigma$ relation. Including (the bulges of) spirals in our reference sample of ellipticals and lenticulars (that of Savorgnan et al. 2016) confirms and extends our results. In this context it is no longer meaningful, at least within the biased samples, to look for outliers in the observed $M_{\text{bh}}-M_{\text{star}}$ relation, such as “pseudo-bulges” (e.g., Kormendy et al. 2011), or examine whether bulge or total luminosity is a better predictor of M_{bh} (e.g., Marconi & Hunt 2003; Häring & Rix 2004; Kormendy & Bender 2011; Läscher et al. 2014), or consider the connection to nuclear star clusters only in terms of stellar mass (e.g., Antonini et al. 2015; Georgiev et al. 2016).

Our Monte Carlo results constrain the normalization of the intrinsic black hole-galaxy scaling relations to be a factor of $\gtrsim 3$ lower than current estimates, in terms of velocity dispersion, and up to a factor of $\sim 50 - 100$ lower when expressing black hole masses as a function of stellar mass (e.g., Figure 3). These results can reconcile the apparent mass discrepancies between local dynamical mass samples and local active galaxies (e.g., our Figure 10), in Narrow Line Seyfert 1 active galaxies (e.g., Orban de Xivry et al. 2011; Sani et al. 2011; Mathur et al. 2012; Shankar et al. 2012a; Calderone et al. 2013, and references therein), moderately luminous AGN (e.g., Ho & Kim 2014; Reines & Volonteri 2015; Ho & Kim 2016; Läscher et al. 2016), active low surface brightness galaxies (Subramanian et al. 2016), and possibly also in more distant samples (Sanghvi et al. 2014; Falomo et al. 2014; Busch et al. 2016).

The lowered normalization of the intrinsic $M_{\text{bh}}-\sigma$ relation will serve as a more secure base for calibrating virial estimators of black hole mass for reverberation mapping-based scaling relations (e.g., Onken et al. 2004; Woo et al. 2010; Graham et al. 2011; Park et al. 2012a; Grier et al. 2013; Ho & Kim 2015). The exact value of f_{vir} , which depends on the structure, dynamics, and line-of-sight orientation of the broad line region, is indeed still a matter of intense debate (see, e.g., Yong et al. 2016, for a recent discussion). Typical values in the literature vary between average values of $f_{\text{vir}} \sim 1$ and $f_{\text{vir}} \sim 4$, depending, respectively, on whether the emission-line profile which enters the virial equation is measured via its full-width at half maximum or its line dispersion (e.g., Collin et al. 2006; Park et al. 2012b; Ho & Kim 2014). Our analysis tends to favour lower values of f_{vir} , i.e. $f_{\text{vir}} \approx 1$ rather than 4. A smaller f_{vir} by itself has a number of interesting consequences. For example, it may ease the challenge of growing very massive black holes in the early Universe (e.g., Mortlock et al. 2011; Trakhtenbrot et al. 2015; Wu et al. 2015), alleviates the need to invoke very massive seeds (e.g., Alexander & Natarajan 2014;

Madau et al. 2014; Lupi et al. 2015), and it may also add some empirical evidence towards the existence of intermediate-mass black holes (e.g., Farrell et al. 2014).

Having lower mass black holes may imply a proportionally lower integrated local black hole mass density (e.g. Tundo et al. 2007; Bernardi et al. 2007; Graham & Driver 2007b; Yu & Lu 2008; Shankar et al. 2009b, 2013a), rather than a factor of a few higher as current estimates based on the (selection biased) $M_{\text{bh}}-M_{\text{star}}$ relation suggest. The most recent accretion models (Shankar et al. 2013b; Aversa et al. 2015), based on Soltan-type (Soltan 1982) arguments and continuity equation models (e.g., Cavaliere et al. 1971; Small & Blandford 1992; Marconi et al. 2004; Yu & Lu 2004), suggest moderate average radiative efficiencies on the order of $\epsilon \lesssim 0.1$. Further increasing the local mass density by a factor of a few, as suggested by the current estimates of the local $M_{\text{bh}}-M_{\text{bulge}}$ relation, would imply a radiative efficiency proportionally lower (Novak 2013), forcing the accretion models towards somewhat extreme scenarios such as frequent radiatively inefficient accretion and/or large fractions of heavily obscured, Compton-thick active galaxies (Comastri et al. 2015). In contrast, a high radiative efficiency would imply that most of the local black holes are spinning rapidly, suggesting that spin may not be the only parameter controlling radio loudness in AGN, in line with many other, independent lines of evidence (e.g., Sikora et al. 2007; Shankar et al. 2008, 2010b, 2016, and references therein).

Finally, lowering the normalization for the intrinsic black hole scaling relations impacts the expected signal in gravitational wave searches (e.g., Sesana et al. 2014, 2016, and references therein). A factor of few reduction in the normalisation reduces the characteristic strain amplitude arising from an incoherent ensemble of gravitational waves, and hence the expected signal-to-noise ratio of the gravitational wave background currently being searched for using pulsar timing arrays (e.g., Sesana 2013; The NANOGrav Collaboration et al. 2015; Rosado et al. 2015; Sesana et al. 2016; Simon & Burke-Spolaor 2016). While this reduction alleviates much of the tension between previous predictions and the lack of a detected signal (e.g., Shannon et al. 2015; Taylor et al. 2016), it also suggests that the detection of gravitational radiation via radio telescopes will be more difficult than previously thought (e.g., Sesana et al. 2016).

5.2 Implications for the co-evolution of black holes and galaxies

In standard models, massive, bulged galaxies, the usual hosts of supermassive black holes, are formed in a highly star-forming, gas-rich phase at early cosmological epochs. A central, “seed” black hole is expected to gradually grow via gas accretion, eventually becoming massive enough to shine as a quasar and trigger powerful winds and/or jets that are capable of removing gas and quenching or inhibiting star formation in the host galaxy (“quasar-mode” and “radio-mode” feedbacks). Feedback from an active black hole has indeed become a key ingredient in many galaxy evolution models (e.g., Granato et al. 2004; Bower et al. 2006; Croton et al. 2006; Monaco et al. 2007; Sijacki et al. 2015). At later times, both the host galaxy and its black hole may further increase their mass (and size) via a sequence of mergers with other galaxies/black holes. Late mergers can contribute up to $\sim 80\%$ of the final mass (e.g., De Lucia et al. 2006; Malbon et al. 2007; Marulli et al. 2008; Naab et al. 2009; Shankar & Bernardi 2009; Oser et al. 2010; Shankar et al. 2010a; González et al. 2011;

Shankar et al. 2013a, 2014, 2015; Zhang et al. 2016; Zhao et al. 2015). The apparent tightness of the $M_{\text{bh}}-M_{\text{star}}$ relation is sometimes used to motivate black hole mass growth by dry mergers (e.g., Peng 2007; Jahnke & Macciò 2011). Such arguments must be reconsidered if this tightness is just a selection effect (Figure 4). Whether merger models can explain the tightness of the $M_{\text{bh}}-\sigma$ relation remains to be seen.

Moreover, our results suggest that (the bulges of) spirals, which are usually not considered to have undergone a substantial phase of late dry mergers (e.g., Huertas-Company et al. 2013; Patel et al. 2013; Huertas-Company et al. 2015), define similar correlations as do ellipticals, thus further pointing to the $M_{\text{bh}}-\sigma$ relation as the dominant correlation. This weakens the motivation for models in which M_{bh} in spirals grows substantially via any secular process unrelated to σ (e.g., Bower et al. 2006; Hopkins & Hernquist 2009; Bournaud et al. 2011; Draper & Ballantyne 2012; Shankar et al. 2012b; Fontanot et al. 2015; Gatti et al. 2016).

The importance of σ inferred from our analysis supports models in which AGN, and in particular quasar-mode feedback, play a key role in linking black holes to their host galaxies. Our results suggest that the scaling with σ is strong, $M_{\text{bh}} \propto \sigma^5$ (Figure 9), typical of energy-driven winds (e.g., Silk & Rees 1998; Granato et al. 2004; Hopkins et al. 2006, but see also Cen 2015). In contrast, momentum-driven winds produce a somewhat weaker trend: $M_{\text{bh}} \propto \sigma^4$, though the exact normalization and slopes predicted by AGN-feedback models as a function of time, mass, and host morphology is still a matter of intense debate (e.g., Fabian 1999; King 2003; Fabian 2012; Faucher-Giguère & Quataert 2012; Gabor & Bournaud 2014; King 2014).

Evolution in scaling relations is a powerful constraint on models (e.g., Merloni et al. 2010). However, our results suggest that searches for evolution in terms of M_{star} are less well-motivated (because the observed $M_{\text{bh}}-M_{\text{bulge}}$ relation is more biased and less fundamental). On the other hand, most analyses based on Soltan-type arguments or direct detections suggest that the $M_{\text{bh}}-\sigma$ relation evolves weakly if at all (e.g., Gaskell & Kormendy 2009; Shankar et al. 2009a; Zhang et al. 2012; Shen et al. 2015, but see also Woo et al. 2008). This further paves the way towards using black holes and quasars as cosmological distance estimators (e.g., Hönig et al. 2014).

Our results shed some light on the long-standing issue regarding the most accurate local black hole mass estimator in favour of the $M_{\text{bh}}-\sigma$ relation (with similar slope but lower normalization, and a possible additional weak dependence on stellar mass). However, this raises a puzzle. Lauer et al. (2007a) argued that the $M_{\text{bh}}-L_{\text{bulge}}$ relation is a more reliable black hole mass estimator for the most massive/luminous galaxies hosting the most massive black holes, such as those in the brightest cluster galaxies (see also, e.g., Laporte & White 2015). They argued that black hole mass estimates via the $M_{\text{bh}}-\sigma$ relation are too low to account for the existence of cores in these galaxies, believed to be produced by the ejection of stars during the decay of black hole binaries. In this respect their conclusions are at odds with our argument that the $M_{\text{bh}}-\sigma$ relation is more fundamental than $M_{\text{bh}}-M_{\text{star}}$. However, our Figure 3 shows that if σ is the driving parameter, then the $M_{\text{bh}}-M_{\text{bulge}}$ relation is at least as biased as the $M_{\text{bh}}-\sigma$ relation, so one should worry about how selection effects affect their argument. In addition, it is possible that other processes such as dynamical friction and AGN feedback effects may contribute to the creation of cores in the inner regions of massive galaxies (e.g., El-Zant et al. 2004; Tonini et al. 2006; Martizzi et al. 2013; El-Zant et al. 2016).

A number of observations and black hole accretion models (e.g., Marconi et al. 2004; Merloni 2004; Granato et al. 2006; Lapi et al. 2006; Zheng et al. 2009; Silverman et al. 2008; Shankar et al. 2009b; Mullaney et al. 2012; Lapi et al. 2014) suggest some degree of correlation between black hole growth and large-scale star formation. On the other hand, a number of observational and theoretical studies are now showing that the actual co-evolution may be more complex to probe observationally, possibly depending on the different evolutionary phases undergone by the host galaxies as well as AGN variability effects (e.g., Hickox et al. 2014; Rodighiero et al. 2015; Volonteri et al. 2015; Graham 2016; Westhues et al. 2016, and references therein). Indeed the large scatter measured in the correlation between star formation and X-ray AGN luminosity (Dai et al. 2015, and references therein) might simply reflect the large scatter in the intrinsic $M_{\text{bh}}-M_{\text{star}}$ relation (Figure 4), a possible independent sign for velocity dispersion, instead of stellar mass, acting as the main driver of the co-evolution between central black holes and their hosts.

How and why galaxies transition from a very active, star-forming phase to a red-and-dead one is still hotly debated. There are a number of hypotheses (not necessarily mutual exclusive) put forward in the literature to explain the quenching of star formation in galaxies (e.g., Woo et al. 2013). Our results on the importance of the $M_{\text{bh}}-\sigma$ relation suggests that the action of black hole feedback triggered during a quasar-like phase may be a substantial contributor to quenching. In this respect, mounting evidence for a nearly environment-independent flattening in the star formation rate-stellar mass relation at high M_{star} (e.g., Erfanianfar et al. 2016, and references therein), paralleling an increased incidence of bulge-dominated galaxies, is also suggestive. The increase in host velocity dispersion may in fact be correlated with the growth of a central black hole; the associated feedback can reduce star formation, though alternative explanations in terms of, e.g., morphological transformations, may still be viable solutions (e.g., Martig et al. 2009; Huertas-Company et al. 2015).

6 CONCLUSIONS

The main aim of this work was to revisit the local scaling relations between black holes and their host galaxies. Our main results can be summarized as follows:

- We have confirmed previous findings that local galaxies with dynamical black hole mass estimates are a biased subset of all galaxies (e.g., Yu & Tremaine 2002; Bernardi et al. 2007; van den Bosch et al. 2015). At fixed stellar mass, local black hole hosts typically have velocity dispersions that are larger than the bulk of the population, irrespective of their exact morphological type or of the aperture within which the velocity dispersion aperture is measured (Figure 1). One of the main reasons for this bias is the observationally imposed requirement that the black hole sphere of influence (equation 2) must be resolved for the black hole mass to be reliably estimated.
- We have confirmed the assertion in Bernardi et al. (2007) that the selection bias cannot be ignored: black hole scaling relations currently in the literature are biased. To properly interpret the measured M_{bh} -scaling relations, one must quantify the effects of this bias. We did so by carrying out Monte Carlo simulations in which we assumed different scaling relations to assign black holes to mock galaxies (equations 4–5), and then applied the r_{infl} -related

selection cuts. These show that the intrinsic relation

$$\log \left(\frac{M_{\text{bh}}}{M_{\odot}} \right) = \gamma + \beta \log \left(\frac{\sigma}{200 \text{ km s}^{-1}} \right) + \alpha \log \left(\frac{M_{\text{star}}}{10^{11} M_{\odot}} \right)$$

with $\gamma = 7.7$, $\beta \sim 4.5 - 5$, $\alpha \lesssim 0.5$, and intrinsic scatter of the order of 0.25 dex reproduces all the observed scaling relations (Figures 3, 5 and 9), as well as the biased relation between velocity dispersion and stellar mass observed in local black hole hosts (Figure 2). Equations (6) and (7) give the $M_{\text{bh}}-M_{\text{star}}$ and $M_{\text{bh}}-\sigma$ relations which result from this $M_{\text{bh}}-\sigma-M_{\text{star}}$ relation.

- The observed $M_{\text{bh}}-M_{\text{star}}$ relation is much more biased than $M_{\text{bh}}-\sigma$ (Figure 3). The apparent tightness of the $M_{\text{bh}}-M_{\text{star}}$ relation is a selection effect, as are trends of the scatter with mass (Figure 4).
- A more detailed comparison of the scaling relations in our selection-biased Monte Carlo samples with similar relations in real data suggest that the correlation with velocity dispersion is the dominant one: any additional dependence on stellar mass and effective radius must be small (Figures 5, 6 and A2–B1).
- Spirals tend to define similar correlations to ellipticals and lenticulars. All our results remain valid if we replace M_{star} with M_{bulge} (Section 4.5; Figures 7, 8 and A1).

Our findings have a number of implications:

- (1) Our preference for steeper slopes in the intrinsic $M_{\text{bh}}-\sigma$ relation ($\beta \gtrsim 5$), is consistent with that of energy-driven AGN feedback models. Our normalization, $\log(M_{\text{bh}}/M_{\odot}) = 7.8$ at $\sigma = 200 \text{ km s}^{-1}$ (Equation 7), is a factor $\gtrsim 3\times$ lower than previous estimates. This suggests proportionally lower black hole mass densities, and so higher radiative efficiencies, supporting a scenario in which most super-massive black holes are rapidly spinning. Reducing M_{bh} values by a factor $\gtrsim 3$ also reduces the predicted gravitational wave signal from black hole mergers, perhaps explaining why pulsar timing arrays have not yet reported detections.
- (2) Our revised intrinsic black hole scaling relations will serve as a more secure base for calibrating virial estimators of black hole mass for reverberation mapping-based scaling relations. Our results suggest that the calibration factor should be reduced to $f_{\text{vir}} \approx 1$.
- (3) The fact that the $M_{\text{bh}}-M_{\text{star}}$ relation is so much more biased than $M_{\text{bh}}-\sigma$ (top panels of Figure 3) explains most of the offset between local (inactive) M_{bh} samples having dynamical mass estimates, and AGN-based samples (Figure 10).
- (4) Our simulations also disfavour broad distributions of black hole masses at fixed velocity dispersion (Figure 11).
- (5) Unless one has accounted for selection effects, looking for outliers (e.g. bars, pseudo-bulges) from the $M_{\text{bh}}-M_{\text{star}}$ relation is no longer so meaningful. Similarly, searches for redshift evolution in the $M_{\text{bh}}-M_{\text{star}}$ relation, which do not account for selection effects, are not well-motivated. Since the apparent tightness and mass dependence of the $M_{\text{bh}}-M_{\text{star}}$ relation are biased by the selection effect, any heavily (dry) merger-driven black hole growth model must be reconsidered.
- (6) The similarity of spirals to ellipticals means that the motivation for models which trigger black holes via disc instabilities or processes other than quasar feedback that do not directly involve velocity dispersion should be re-evaluated.
- (7) As σ is the controlling parameter in a number of other galaxy scaling relations (Bernardi et al. 2005), our finding that σ is the most important parameter in M_{bh} scaling relations will serve as a more robust test for the next generation of galaxy-black hole co-evolution models, for a deeper understanding of high-redshift data on active and star-forming galaxies, and for more accurate estimates of the black hole mass function.

ACKNOWLEDGMENTS

FS warmly thanks S. Ottavi for her invaluable and constant support. We thank A. Beifiori for sharing her data in electronic format and for helpful clarifications on some of the samples considered in this work. We thank an anonymous referee for helpful suggestions that improved the presentation of our results. FS also thanks N. McConnell, P. Monaco, A. Reines, and M. Volonteri for useful discussions.

REFERENCES

- Abazajian K. N. et al., 2009, *ApJS*, 182, 543
- Aguerrri J. A. L., Balcells M., Peletier R. F., 2001, *A&A*, 367, 428
- Alexander T., Natarajan P., 2014, *Science*, 345, 1330
- Aller M. C., Richstone D., 2002, *AJ*, 124, 3035
- Antonini F., Barausse E., Silk J., 2015, *ApJ*, 812, 72
- Arnold J. A. et al., 2014, *ApJ*, 791, 80
- Aversa R., Lapi A., de Zotti G., Shankar F., Danese L., 2015, *ApJ*, 810, 74
- Baes M., Buyle P., Hau G. K. T., Dejonghe H., 2003, *MNRAS*, 341, L44
- Barth A. J., 2004, 222, 3
- Batcheldor D., 2010, *ApJ*, 711, L108
- Beifiori A., Courteau S., Corsini E. M., Zhu Y., 2012, *MNRAS*, 419, 2497
- Beifiori A., Sarzi M., Corsini E. M., Dalla Bontà E., Pizzella A., Coccato L., Bertola F., 2009, *ApJ*, 692, 856
- Bekenstein J. D., 1973, *ApJ*, 183, 657
- Bell E. F., McIntosh D. H., Katz N., Weinberg M. D., 2003, *ApJS*, 149, 289
- Benson A. J., Džanović D., Frenk C. S., Sharples R., 2007, *MNRAS*, 379, 841
- Bernardi M., Meert A., Sheth R. K., Fischer J.-L., Huertas-Company M., Maraston C., Shankar F., Vikram V., 2016a, *ArXiv:1604.01036*
- Bernardi M., Meert A., Sheth R. K., Huertas-Company M., Maraston C., Shankar F., Vikram V., 2016b, *MNRAS*, 455, 4122
- Bernardi M., Meert A., Sheth R. K., Vikram V., Huertas-Company M., Mei S., Shankar F., 2013, *MNRAS*, 436, 697
- Bernardi M., Meert A., Vikram V., Huertas-Company M., Mei S., Shankar F., Sheth R. K., 2014, *MNRAS*, 443, 874
- Bernardi M., Roche N., Shankar F., Sheth R. K., 2011, *MNRAS*, 412, 684
- Bernardi M., Shankar F., Hyde J. B., Mei S., Marulli F., Sheth R. K., 2010, *MNRAS*, 404, 2087
- Bernardi M., Sheth R. K., Nichol R. C., Schneider D. P., Brinkmann J., 2005, *AJ*, 129, 61
- Bernardi M., Sheth R. K., Tundo E., Hyde J. B., 2007, *ApJ*, 660, 267
- Berti E., Cardoso V., Starinets A. O., 2009, *Classical and Quantum Gravity*, 26, 163001
- Bogdán Á., Goulding A. D., 2015, *ApJ*, 800, 124
- Bonnor W. B., Rotenberg M. A., 1961, *Proceedings of the Royal Society of London Series A*, 265, 109
- Bournaud F., Dekel A., Teyssier R., Cacciato M., Daddi E., Juneau S., Shankar F., 2011, *ApJ*, 741, L33
- Bower R. G., Benson A. J., Malbon R., Helly J. C., Frenk C. S., Baugh C. M., Cole S., Lacey C. G., 2006, *MNRAS*, 370, 645
- Boylan-Kolchin M., Ma C.-P., Quataert E., 2006, *MNRAS*, 369, 1081
- Bruzual G., Charlot S., 2003, *MNRAS*, 344, 1000
- Buonanno A., Damour T., 2000, *Phys. Rev. D*, 62, 064015
- Busch G. et al., 2016, *A&A*, 587, A138
- Calderone G., Ghisellini G., Colpi M., Dotti M., 2013, *MNRAS*, 431, 210
- Cappellari M. et al., 2006, *MNRAS*, 366, 1126
- Cappellari M. et al., 2013, *MNRAS*, 432, 1862
- Cavaliere A., Morrison P., Wood K., 1971, *ApJ*, 170, 223
- Cen R., 2015, *ApJ*, 805, L9
- Chabrier G., 2003, *PASP*, 115, 763
- Collin S., Kawaguchi T., Peterson B. M., Vestergaard M., 2006, *A&A*, 456, 75
- Comastri A., Gilli R., Marconi A., Risaliti G., Salvati M., 2015, *A&A*, 574, L10
- Croton D. J. et al., 2006, *MNRAS*, 365, 11
- Dai Y. S., Wilkes B. J., Bergeron J., Omont A., Kuraszkiewicz J., Teplitz H. I., 2015, *ArXiv:1511.06761*
- De Lucia G., Springel V., White S. D. M., Croton D., Kauffmann G., 2006, *MNRAS*, 366, 499
- Delvecchio I. et al., 2014, *MNRAS*, 439, 2736
- Draper A. R., Ballantyne D. R., 2012, *ApJ*, 751, 72
- Dubois Y., Gavazzi R., Peirani S., Silk J., 2013, *MNRAS*, 433, 3297
- Dullo B. T., Graham A. W., 2015, *ApJ*, 798, 55
- El-Zant A., Freundlich J., Combes F., 2016, *ArXiv:1603.00526*
- El-Zant A. A., Hoffman Y., Primack J., Combes F., Shlosman I., 2004, *ApJ*, 607, L75
- Elvis M., Risaliti G., Zamorani G., 2002, *ApJ*, 565, L75
- Erfanianfar G. et al., 2016, *MNRAS*, 455, 2839
- Faber S. M., 1999, *Advances in Space Research*, 23, 925
- Fabian A. C., 1999, *MNRAS*, 308, L39
- Fabian A. C., 2012, *ARA&A*, 50, 455
- Falomo R., Bettoni D., Karhunen K., Kotilainen J. K., Uslenghi M., 2014, *MNRAS*, 440, 476
- Fanidakis N., Baugh C. M., Benson A. J., Bower R. G., Cole S., Done C., Frenk C. S., 2011, *MNRAS*, 410, 53
- Farrell S. A. et al., 2014, *MNRAS*, 437, 1208
- Farrell S. A., Webb N. A., Barret D., Godet O., Rodrigues J. M., 2009, *Nature*, 460, 73
- Faucher-Giguère C.-A., Quataert E., 2012, *MNRAS*, 425, 605
- Feoli A., Mele D., 2005, *International Journal of Modern Physics D*, 14, 1861
- Ferrarese L., 2002a, *ApJ*, 578, 90
- Ferrarese L., 2002b, in *Current High-Energy Emission Around Black Holes*, Lee C.-H., Chang H.-Y., eds., pp. 3–24
- Ferrarese L., Ford H., 2005, *Space Science Reviews*, 116, 523
- Ferrarese L., Merritt D., 2000, *ApJ*, 539, L9
- Fontana F., Monaco P., Cristiani S., Tozzi P., 2006, *MNRAS*, 373, 1173
- Fontana F., Monaco P., Shankar F., 2015, *MNRAS*, 453, 4112
- Ford H. C., Tsvetanov Z. I., Ferrarese L., Jaffe W., 1998, in *IAU Symposium, Vol. 184, The Central Regions of the Galaxy and Galaxies*, Sofue Y., ed., p. 377
- Gabor J. M., Bournaud F., 2014, *MNRAS*, 441, 1615
- Gaskell C. M., Kormendy J., 2009, *ArXiv:0907.1652*
- Gatti M., Shankar F., Bouillot V., Menci N., Lamastra A., Hirschmann M., Fiore F., 2016, *MNRAS*, 456, 1073
- Gebhardt K., et al., 2000, *ApJ*, 539, L13
- Georgiev I. Y., Böker T., Leigh N., Lützgendorf N., Neumayer N., 2016, *ArXiv:1601.02613*
- González J. E., Lacey C. G., Baugh C. M., Frenk C. S., 2011, *MNRAS*, 412, 128
- Graham A., Colless M., 1997, *MNRAS*, 287, 221
- Graham A. W., 2007, *MNRAS*, 379, 711
- Graham A. W., 2008, *ApJ*, 680, 143
- Graham A. W., 2012, *ApJ*, 746, 113
- Graham A. W., 2016, *Galactic Bulges*, 418, 263
- Graham A. W., Driver S. P., 2007a, *ApJ*, 655, 77
- Graham A. W., Driver S. P., 2007b, *MNRAS*, 380, L15
- Graham A. W., Driver S. P., Allen P. D., Liske J., 2007, *MNRAS*, 378, 198
- Graham A. W., Erwin P., Caon N., Trujillo I., 2001, *ApJ*, 563, L11
- Graham A. W., Onken C. A., Athanassoula E., Combes F., 2011, *MNRAS*, 412, 2211
- Graham A. W., Scott N., 2013, *ApJ*, 764, 151
- Graham A. W., Scott N., 2015, *ApJ*, 798, 54
- Granato G. L., De Zotti G., Silva L., Bressan A., Danese L., 2004, *ApJ*, 600, 580
- Granato G. L., Silva L., Lapi A., Shankar F., De Zotti G., Danese L., 2006, *MNRAS*, 368, L72
- Grier C. J. et al., 2013, *ApJ*, 773, 90
- Gültekin K. et al., 2009, *ApJ*, 698, 198
- Gültekin K., Tremaine S., Loeb A., Richstone D. O., 2011, *ApJ*, 738, 17
- Håring N., Rix H.-W., 2004, *ApJ*, 604, L89

- Hickox R. C., Mullaney J. R., Alexander D. M., Chen C.-T. J., Civano F. M., Goulding A. D., Hainline K. N., 2014, *ApJ*, 782, 9
- Hilz M., Naab T., Ostriker J. P., 2013, *MNRAS*, 429, 2924
- Hirschmann M., Dolag K., Saro A., Bachmann L., Borgani S., Burkert A., 2014, *MNRAS*, 442, 2304
- Hirschmann M., Khochfar S., Burkert A., Naab T., Genel S., Somerville R. S., 2010, *MNRAS*, 407, 1016
- Ho L., Kim M., 2016, *ArXiv:1603.00057*
- Ho L. C., Kim M., 2014, *ApJ*, 789, 17
- Ho L. C., Kim M., 2015, *ApJ*, 809, 123
- Hobbs G. et al., 2010, *Classical and Quantum Gravity*, 27, 084013
- Hönig S. F., Watson D., Kishimoto M., Hjorth J., 2014, *Nature*, 515, 528
- Hopkins P. F., Hernquist L., 2009, *ApJ*, 694, 599
- Hopkins P. F., Hernquist L., Cox T. J., Di Matteo T., Robertson B., Springel V., 2006, *ApJS*, 163, 1
- Hopkins P. F., Hernquist L., Cox T. J., Robertson B., Krause E., 2007, *ApJ*, 669, 67
- Huertas-Company M., Aguerri J. A. L., Bernardi M., Mei S., Sánchez Almeida J., 2011, *A&A*, 525, A157
- Huertas-Company M. et al., 2015, *ApJ*, 809, 95
- Huertas-Company M., Shankar F., Mei S., Bernardi M., Aguerri J. A. L., Meert A., Vikram V., 2013, *ApJ*, 779, 29
- Jahnke K., Macciò A. V., 2011, *ApJ*, 734, 92
- Jorgensen I., Franx M., Kjaergaard P., 1996, *MNRAS*, 280, 167
- Kauffmann G., Haehnelt M., 2000, *MNRAS*, 311, 576
- King A., 2003, *ApJ*, 596, L27
- King A., 2005, *ApJ*, 635, L121
- King A., 2014, *Space Sci. Rev.*, 183, 427
- Kormendy J., Bender R., 2011, *Nature*, 469, 377
- Kormendy J., Bender R., Cornell M. E., 2011, *Nature*, 469, 374
- Kormendy J., Ho L. C., 2013, *ARA&A*, 51, 511
- Kramer M., Champion D. J., 2013, *Classical and Quantum Gravity*, 30, 224009
- Kroupa P., 2001, *MNRAS*, 322, 231
- Lapi A., Raimundo S., Aversa R., Cai Z.-Y., Negrello M., Celotti A., De Zotti G., Danese L., 2014, *ApJ*, 782, 69
- Lapi A., Shankar F., Mao J., Granato G. L., Silva L., De Zotti G., Danese L., 2006, *ApJ*, 650, 42
- Laporte C. F. P., White S. D. M., 2015, *MNRAS*, 451, 1177
- Läsker R., Ferrarese L., van de Ven G., Shankar F., 2014, *ApJ*, 780, 70
- Läsker R., Greene J. E., Seth A., van de Ven G., Braatz J. A., Henkel C., Lo K. Y., 2016, *ArXiv:1602.06960*
- Lauer T. R. et al., 2007a, *ApJ*, 662, 808
- Lauer T. R., Tremaine S., Richstone D., Faber S. M., 2007b, *ApJ*, 670, 249
- Licquia T. C., Newman J. A., 2015, *ApJ*, 806, 96
- Longhetti M., Saracco P., 2009, *MNRAS*, 394, 774
- Lupi A., Haardt F., Dotti M., Fiacconi D., Mayer L., Madau P., 2015, *ArXiv:1512.02651*
- Madau P., Haardt F., Dotti M., 2014, *ApJ*, 784, L38
- Magorrian J. et al., 1998, *AJ*, 115, 2285
- Malbon R. K., Baugh C. M., Frenk C. S., Lacey C. G., 2007, *MNRAS*, 382, 1394
- Marconi A., Hunt L. K., 2003, *ApJ*, 589, L21
- Marconi A., Risaliti G., Gilli R., Hunt L. K., Maiolino R., Salvati M., 2004, *MNRAS*, 351, 169
- Martig M., Bournaud F., Teyssier R., Dekel A., 2009, *ApJ*, 707, 250
- Martizzi D., Teyssier R., Moore B., 2013, *MNRAS*, 432, 1947
- Marulli F., Bonoli S., Branchini E., Moscardini L., Springel V., 2008, *MNRAS*, 385, 1846
- Mathur S., Fields D., Peterson B. M., Grupe D., 2012, *ApJ*, 754, 146
- McConnell N. J., Ma C.-P., 2013, *ApJ*, 764, 184
- McLure R. J., Dunlop J. S., 2004, *MNRAS*, 352, 1390
- Meert A., Vikram V., Bernardi M., 2013, *MNRAS*, 433, 1344
- Meert A., Vikram V., Bernardi M., 2015, *MNRAS*, 446, 3943
- Meidt S. E. et al., 2014, *ApJ*, 788, 144
- Menci N., Fontana A., Giallongo E., Grazian A., Salimbeni S., 2006, *ApJ*, 647, 753
- Merloni A., 2004, *MNRAS*, 353, 1035
- Merloni A. et al., 2010, *ApJ*, 708, 137
- Merritt D., 2006, *ApJ*, 648, 976
- Merritt D., 2013, *Dynamics and Evolution of Galactic Nuclei*
- Merritt D., Ferrarese L., 2001a, in *Astronomical Society of the Pacific Conference Series*, Vol. 249, *The Central Kiloparsec of Starbursts and AGN: The La Palma Connection*, Knapen J. H., Beckman J. E., Shlosman I., Mahoney T. J., eds., p. 335
- Merritt D., Ferrarese L., 2001b, *ApJ*, 547, 140
- Mezcua M., Civano F., Fabbiano G., Miyaji T., Marchesi S., 2015, *ArXiv:151105844*
- Monaco P., Fontanot F., Taffoni G., 2007, *MNRAS*, 375, 1189
- Morabito L. K., Dai X., 2012, *ApJ*, 757, 172
- Mortlock D. J. et al., 2011, *Nature*, 474, 616
- Mullaney J. R. et al., 2012, *ApJ*, 753, L30
- Naab T., Johansson P. H., Ostriker J. P., 2009, *ApJ*, 699, L178
- Novak G. S., 2013, *ArXiv:1310.3833*
- Novak G. S., Faber S. M., Dekel A., 2006, *ApJ*, 637, 96
- Onken C. A., Ferrarese L., Merritt D., Peterson B. M., Pogge R. W., Vestergaard M., Wandel A., 2004, *ApJ*, 615, 645
- Orban de Xivry G., Davies R., Schartmann M., Komossa S., Marconi A., Hicks E., Engel H., Tacconi L., 2011, *MNRAS*, 417, 2721
- Oser L., Ostriker J. P., Naab T., Johansson P. H., Burkert A., 2010, *ApJ*, 725, 2312
- Park D., Kelly B. C., Woo J.-H., Treu T., 2012a, *ApJS*, 203, 6
- Park D. et al., 2012b, *ApJ*, 747, 30
- Patel S. G. et al., 2013, *ApJ*, 778, 115
- Paturel G., Petit C., Prugniel P., Theureau G., Rousseau J., Brouty M., Dubois P., Cambrésy L., 2003, *A&A*, 412, 45
- Peebles P. J. E., 1972, *General Relativity and Gravitation*, 3, 63
- Peng C. Y., 2007, *ApJ*, 671, 1098
- Peres A., 1962, *Physical Review*, 128, 2471
- Ravi V., Wyithe J. S. B., Shannon R. M., Hobbs G., Manchester R. N., 2014, *MNRAS*, 442, 56
- Reines A. E., Volonteri M., 2015, *ApJ*, 813, 82
- Richstone D. et al., 1998, *Nature*, 395, A14+
- Rodighiero G. et al., 2015, *ApJ*, 800, L10
- Rosado P. A., Sesana A., 2014, *MNRAS*, 439, 3986
- Rosado P. A., Sesana A., Gair J., 2015, *MNRAS*, 451, 2417
- Rusli S. P. et al., 2013, *AJ*, 146, 45
- Sabra B. M., Saliba C., Abi Akl M., Chahine G., 2015, *ApJ*, 803, 5
- Saglia R. P. et al., 2016, *ApJ*, 818, 47
- Salucci P., Szuszkiewicz E., Monaco P., Danese L., 1999, *MNRAS*, 307, 637
- Sanghvi J., Kotilainen J. K., Falomo R., Decarli R., Karhunen K., Uslenghi M., 2014, *MNRAS*, 445, 1261
- Sani E., Marconi A., Hunt L. K., Risaliti G., 2011, *MNRAS*, 413, 1479
- Satyapal S., Vega D., Dudik R. P., Abel N. P., Heckman T., 2008, *ApJ*, 677, 926
- Savorgnan G. A. D., Graham A. W., 2015a, *MNRAS*, 446, 2330
- Savorgnan G. A. D., Graham A. W., 2015b, *ArXiv:151107446*
- Savorgnan G. A. D., Graham A. W., Marconi A., Sani E., 2016, *ApJ*, 817, 21
- Schulze A. et al., 2015, *MNRAS*, 447, 2085
- Schulze A., Wisotzki L., 2011, *A&A*, 535, A87
- Schulze A., Wisotzki L., 2014, *MNRAS*, 438, 3422
- Scott N., Graham A. W., Schombert J., 2013, *ApJ*, 768, 76
- Sérsic J. L., 1963, *Boletín de la Asociación Argentina de Astronomía La Plata Argentina*, 6, 41
- Sesana A., 2013, *MNRAS*, 433, L1
- Sesana A., Barausse E., Dotti M., Rossi E. M., 2014, *ApJ*, 794, 104
- Sesana A., Shankar F., Bernardi M., Sheth R. K., 2016, *ArXiv e-prints*
- Sesana A., Vecchio A., Colacino C. N., 2008, *MNRAS*, 390, 192
- Shankar F., 2009, *New Astron. Rev.*, 53, 57
- Shankar F., Bernardi M., 2009, *MNRAS*, 396, L76
- Shankar F., Bernardi M., Haiman Z., 2009a, *ApJ*, 694, 867
- Shankar F. et al., 2015, *ApJ*, 802, 73
- Shankar F. et al., 2016, *ApJ*, 818, L1
- Shankar F., Cavaliere A., Cirasuolo M., Maraschi L., 2008, *ApJ*, 676, 131

Shankar F., Marulli F., Bernardi M., Boylan-Kolchin M., Dai X., Khochfar S., 2010a, MNRAS, 405, 948

Shankar F., Marulli F., Bernardi M., Mei S., Meert A., Vikram V., 2013a, MNRAS, 428, 109

Shankar F., Marulli F., Mathur S., Bernardi M., Bournaud F., 2012a, A&A, 540, A23

Shankar F., Marulli F., Mathur S., Bernardi M., Bournaud F., 2012b, A&A, 540, A23

Shankar F. et al., 2014, MNRAS, 439, 3189

Shankar F., Salucci P., Granato G. L., De Zotti G., Danese L., 2004, MNRAS, 354, 1020

Shankar F., Sivakoff G. R., Vestergaard M., Dai X., 2010b, MNRAS, 401, 1869

Shankar F., Weinberg D. H., Miralda-Escudé J., 2009b, ApJ, 690, 20

Shankar F., Weinberg D. H., Miralda-Escudé J., 2013b, MNRAS, 428, 421

Shannon R. M. et al., 2013, Science, 342, 334

Shannon R. M. et al., 2015, Science, 349, 1522

Shen Y. et al., 2015, ApJ, 805, 96

Sheth R. K., Bernardi M., 2012, MNRAS, 422, 1825

Shields G. A., Menezes K. L., Massart C. A., Vanden Bout P., 2006, ApJ, 641, 683

Sijacki D., Vogelsberger M., Genel S., Springel V., Torrey P., Snyder G. F., Nelson D., Hernquist L., 2015, MNRAS, 452, 575

Sikora M., Stawarz Ł., Lasota J.-P., 2007, ApJ, 658, 815

Silk J., Rees M. J., 1998, A&A, 331, L1

Silverman J. D. et al., 2008, ApJ, 679, 118

Simon J., Burke-Spolaor S., 2016, ArXiv:1603.06577

Small T. A., Blandford R. D., 1992, MNRAS, 259, 725

Soltan A., 1982, MNRAS, 200, 115

Subramanian S., Ramya S., Das M., George K., Sivarani T., Prabhu T. P., 2016, MNRAS, 455, 3148

Taylor S. R., Vallisneri M., Ellis J. A., Mingarelli C. M. F., Lazio T. J. W., van Haasteren R., 2016, ApJ, 819, L6

The NANOGrav Collaboration et al., 2015, ApJ, 813, 65

Tonini C., Lapi A., Salucci P., 2006, ApJ, 649, 591

Trakhtenbrot B. et al., 2015, Science, 349, 168

Treu T., Woo J.-H., Malkan M. A., Blandford R. D., 2007, ApJ, 667, 117

Tucci M., Volonteri M., 2016, ArXiv:1603.00823

Tundo E., Bernardi M., Hyde J. B., Sheth R. K., Pizzella A., 2007, ApJ, 663, 53

van den Bosch R. C. E., Gebhardt K., Gültekin K., Yıldırım A., Walsh J. L., 2015, ApJS, 218, 10

Vestergaard M., Peterson B. M., 2006, ApJ, 641, 689

Vika M., Driver S. P., Graham A. W., Liske J., 2009, MNRAS, 400, 1451

Vittorini V., Shankar F., Cavaliere A., 2005, MNRAS, 363, 1376

Vogelsberger M. et al., 2014, MNRAS, 444, 1518

Volonteri M., Capelo P. R., Netzer H., Bellovary J., Dotti M., Governato F., 2015, MNRAS, 452, L6

Webb N. A., Godet O., Wiersema K., Lasota J.-P., Barret D., Farrell S. A., Maccarone T. J., Servillat M., 2014, ApJ, 780, L9

Westhues C. et al., 2016, ArXiv:1602.07443

Woo J. et al., 2013, MNRAS, 428, 3306

Woo J.-H. et al., 2010, ApJ, 716, 269

Woo J.-H., Treu T., Malkan M. A., Blandford R. D., 2008, ApJ, 681, 925

Wu X.-B. et al., 2015, Nature, 518, 512

Wyithe J. S. B., Loeb A., 2005, ApJ, 634, 910

Yong S. Y., Webster R. L., King A. L., 2016, ArXiv:1602.04672

Yu Q., Lu Y., 2004, ApJ, 602, 603

Yu Q., Lu Y., 2008, ApJ, 689, 732

Yu Q., Tremaine S., 2002, MNRAS, 335, 965

Zhang X., Lu Y., Yu Q., 2012, ApJ, 761, 5

Zhang Y. et al., 2016, ApJ, 816, 98

Zhao D., Aragón-Salamanca A., Conselice C. J., 2015, MNRAS, 453, 4444

Zheng X. Z. et al., 2009, ApJ, 707, 1566

APPENDIX A: RESIDUALS IN OTHER DATA SETS

Figures A1, A2, A3, and A4 show correlations between the residuals from scaling relations measured in the samples of Saglia et al. (2016), McConnell & Ma (2013), Läscher et al. (2014), and Beifiori et al. (2012) (the latter with black hole masses taken from Kormendy & Ho (2013)). Figure A1 shows the residuals using bulge luminosities and effective radii in the Saglia et al. (2016) sample, excluding non-barred spirals, while all other samples refer to total stellar masses and effective radii of E+S0s (bulge properties are not available for most of these samples). The grey bands show the corresponding correlations for Model I. In the panels on the left, all data sets define comparable if not even tighter correlations than those shown in Figure 5, while those on the right show weaker dependence on any other variable, in excellent agreement with Model I.

APPENDIX B: RESIDUALS IN Model III

In Model III, the intrinsic relation is $M_{\text{bh}} \propto M_{\text{star}}^2/R_e$, so residuals from correlations with velocity dispersion should be uncorrelated. The grey band in the top left panel of Figure B1 shows this is also true in the selection biased sample. In contrast, the Savorgnan et al. (2016) data show a strong correlation. The data shows a steeper correlation in the bottom left panel as well. On the other hand, in the top right panel, it is the model which shows a stronger correlation than the data. The slopes of these correlations, with uncertainties derived from many Monte Carlo realizations (see Section 4.5), are reported in Table 1.

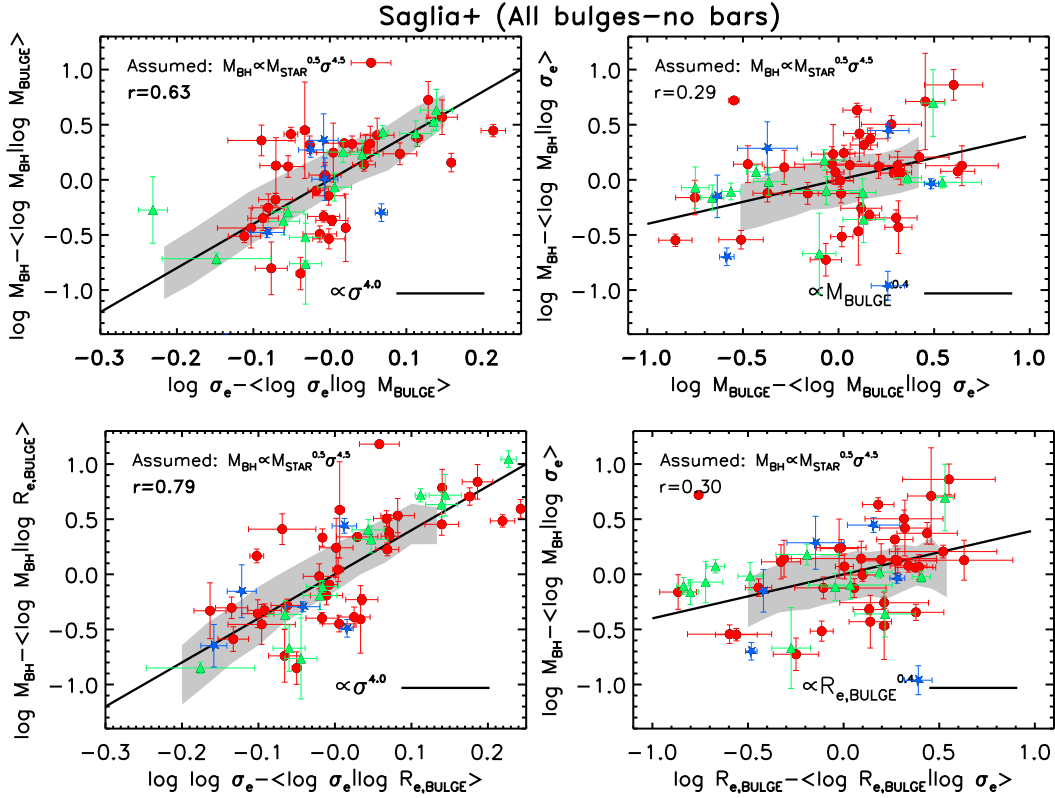


Figure A1. Same as Figure 8, but for bulge stellar masses and half-light radii from Saglia et al. (2016). Red circles indicate barred galaxies, while the colour coding is otherwise the same as in Figure 8.

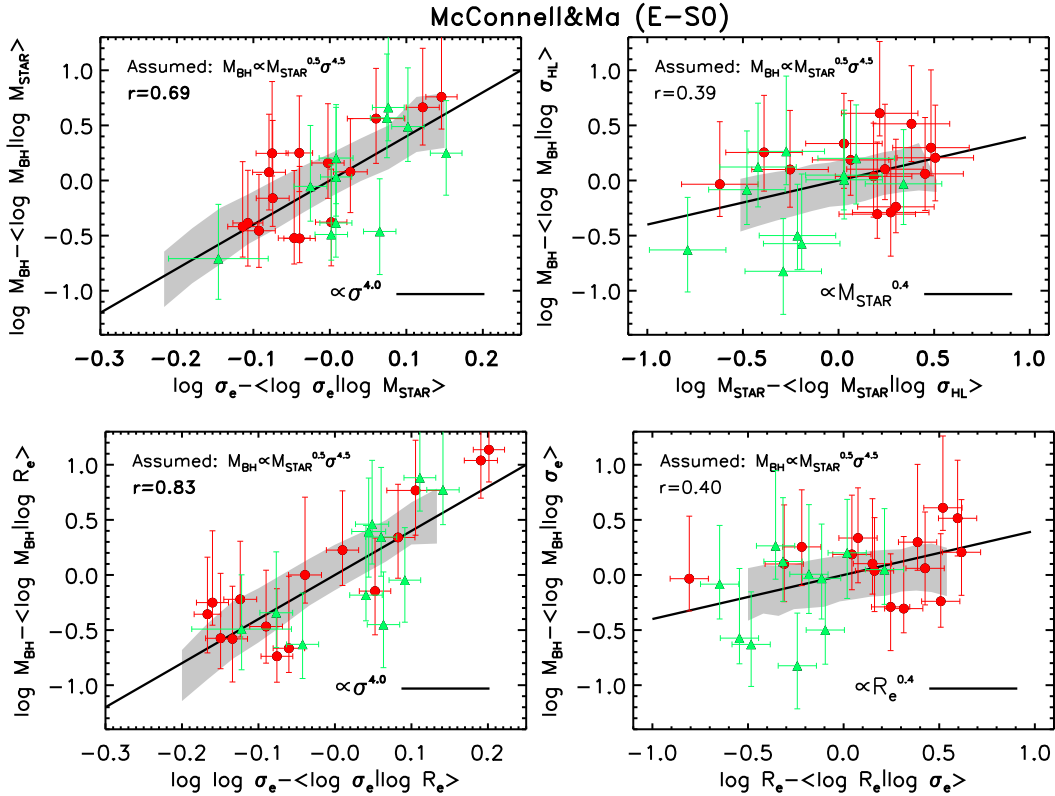


Figure A2. Same as Figure 5 but using the E+S0 sample from Läscher et al. (2014). The data are consistent with velocity dispersion being the most fundamental property connecting black holes to galaxies.

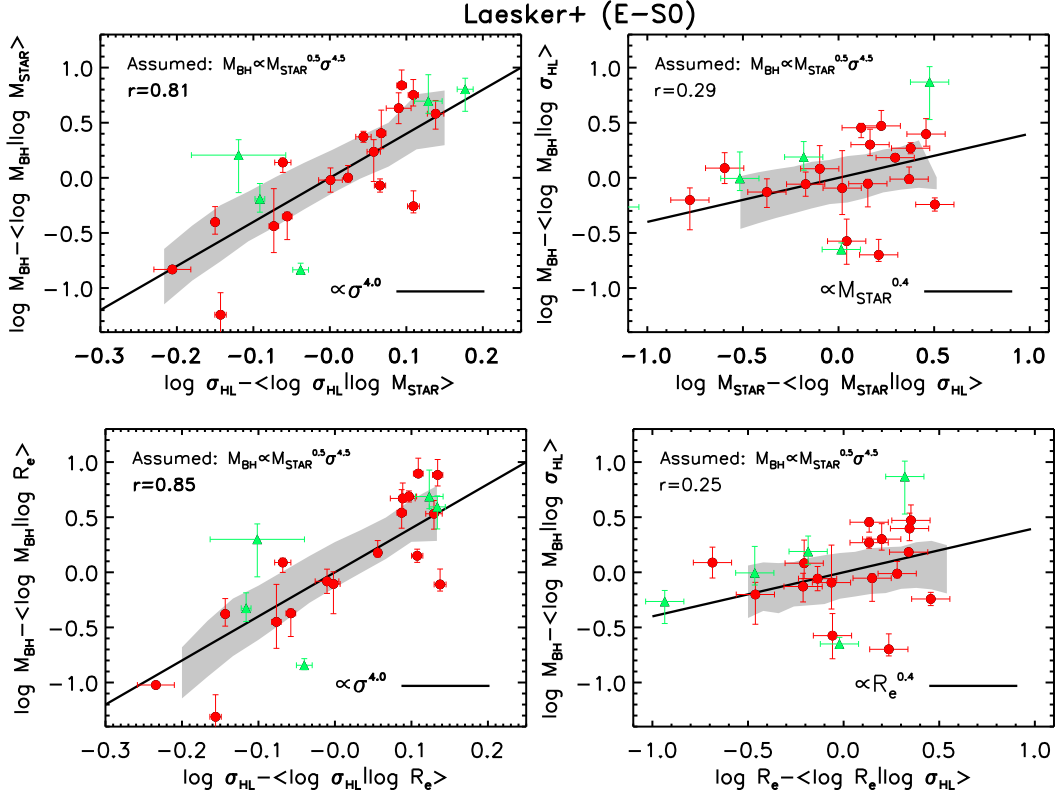


Figure A3. Same as Figure 5 but using the E+S0 sample from Läscher et al. (2014). The data are consistent with velocity dispersion being the most fundamental property connecting black holes to galaxies.

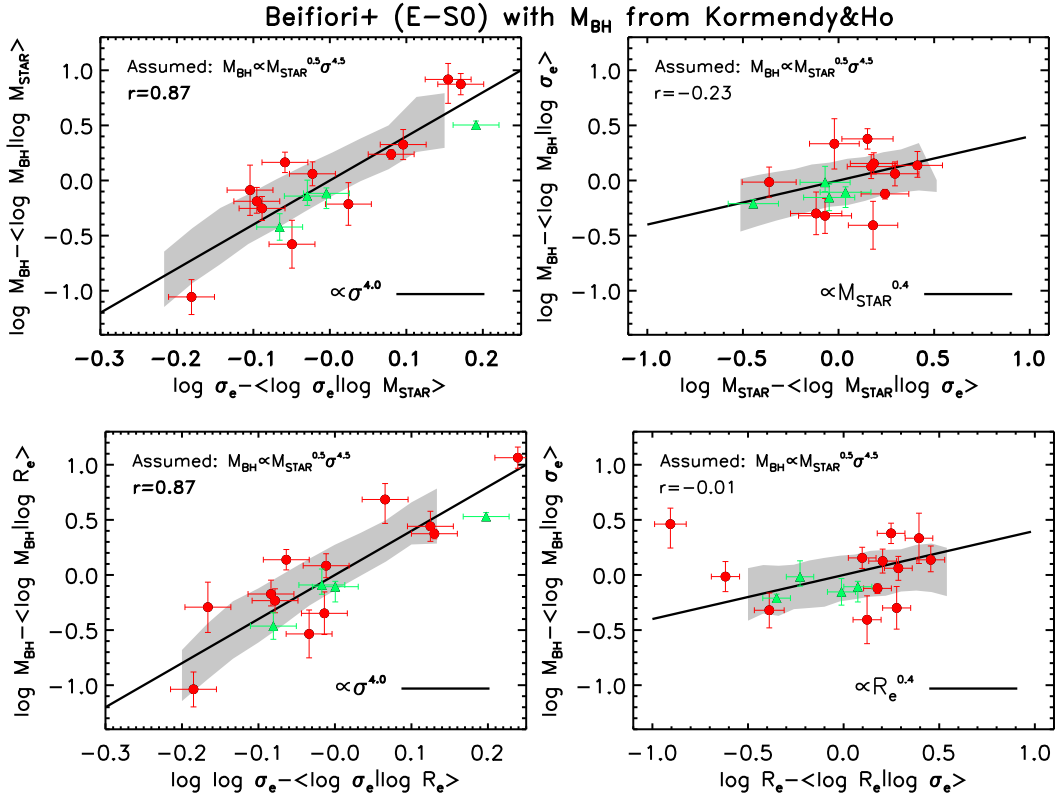


Figure A4. Same as Figure 5 but using the E+S0 sample from McConnell & Ma (2013) with galaxy 3.6μ galaxy luminosities and effective radii from Sani et al. (2011). The data continue being consistent with velocity dispersion being the most fundamental property connecting black holes to galaxies.

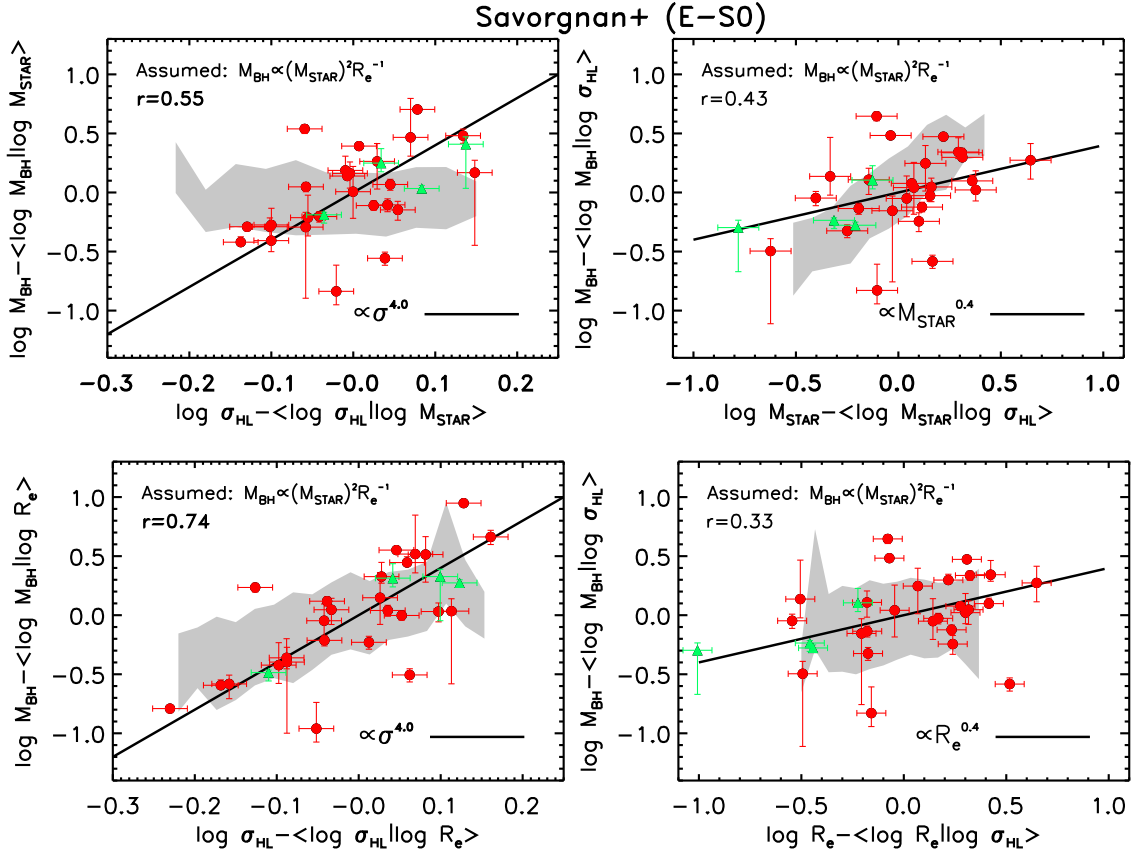


Figure B1. Same as Figure 5 but for Model III. Similarly to Model II, this model also predicts weaker correlations with σ and stronger trends with other variables than is observed.